European Research Infrastructure Supporting Smart Grid Systems Technology Development, Validation and Roll Out

Technical Report TA User Project

Asynchronized Synchronous Motor based Shipboard Power System for All Electric Ship

Grant Agreement No:	**654113**
Funding Instrument:	**Research and Innovation Actions (RIA) – Integrating Activity (IA)**
Funded under:	**INFRAIA-1-2014/2015: Integrating and opening existing national and regional research infrastructures of European interest**
Starting date of project:	**01.11.2015**
Project Duration:	**54 month**

Delivery date:	**28.01.2019**
Name of lead beneficiary for this deliverable:	**Kai Ni, University of Liverpool**
Deliverable Type:	**Report (R)**
Security Class:	**Public (PU)**
Revision / Status:	**Released**

Project co-funded by the European Commission within the H2020 Programme (2014-2020)

Document Information

Document Version:	3
Revision / Status:	Released
All Authors/Partners	Kai Ni, Lujia Xie (University of Liverpool); Dimitris Lagos (ICCS-NTUA)
Distribution List	Public

Document History

Revision	Content / Changes	Resp. Partner	Date
1	Description of the asynchronized synchronous motor (ASM) based shipboard power system (SPS), modelling process in RTDS software, control strategies, and results obtained	Kai Ni, University of Liverpool	19.11.2018
2	Revisions on the details of the report	Lujia Xie, University of Liverpool	21.11.2018
3	Final Version	Kai Ni, University of Liverpool; Dimitris Lagos, ICCS-NTUA	28.01.2019

Document Approval

Final Approval	Name	Resp. Partner	Date
Review and improvements	Dimitris Lagos	ICCS-NTUA	15.01.2019

Disclaimer

Copyright Notice

Table of contents

Abbreviations

AC	Alternation Current
AES	All Electric Ship
ASM	Asynchronized Synchronous Motor
BTB	back-to-back
CHIL	Control-Hardware-in-the-Loop
CI	Computational Intelligence
CPL	Constant Power Load
DC	Direct Current
EMF	Electromagnetic Force
EMS	Energy Management System
GHG	Greenhouse Gas
GSC	Grid-Side Converter
GVO	Grid Voltage Orientation
IMU	Impedance Measurement Unit
IPS	Integrated Power System
ISCPM	Integrated Security-Constrained Power Management
MAS	Multi-Agent System
MMC	Modular Multilevel Converter
MPC	Model Predictive Control
MVDC	Medium Voltage Direct Current
PC	Personal Computer
PEBB	Power Electronics Building Block
PI	Proportional-Integral
PLL	Phase-Locked Loop
PSO	Particle Swarm Optimization
PV	Photovoltaic
RSC	Rotor-Side Converter
RTDS	Real-Time Digital Simulator
SG	Synchronous Generator
SPS	Shipboard Power System
UoL	University of Liverpool
VSC	Voltage Source Converter

Executive Summary

Extensive electrification of ships has been carried out to put forward a novel concept of all electric ship (AES), which caters to the requirements of reducing fuel consumption and increasing the on-board power utilization rate. The normal operation of a commonly used fully decoupled shipboard power system (SPS) depends on power electronic devices, which are fragile and easy to break down. Once a short circuit fault happens in a DC system, enormous currents can be produced that may paralyze the whole SPS. In addition, since most of the power onboard is utilized for propulsion, which is an AC load, there is no need to fully decouple the generated power. Therefore, an asynchronized synchronous motor (ASM) based SPS is proposed to solve the aforementioned problems. In this system, a synchronous generator (SG) is used to supply power to the system, and an ASM is employed to drag the propeller. By applying the ASM-based SPS, only partial generated power is decoupled to deal with a small degree of power unbalance between the power source and load. In this case, the volume of power electronic converter is obviously reduced, which minimizes unnecessary power conversion and increases the system robustness to power converter faults.

In the proposed work, the power circuits of SG and back-to-back (BTB) converter are built up in real-time digital simulator (RTDS) software, with the rotor of ASM simulated as a three-phase voltage source. The synchronous angular frequency and angle are obtained by using a phase-locked loop (PLL) for the three-phase stator voltages of SG, and the rotor angular speed and angle of ASM are derived by PLL with the slip frequency. The IEEE Type 1 excitation system and a governor are used in RTDS software to control the operation of SG. The Park and Inverse Park Transformation blocks are established in RTDS software, while the control blocks for BTB converter in the dq reference frame are built up in Simulink and implemented in the control-hardware-in-the-loop (CHIL) setup. During the stay in ICCS-NTUA, the normal operation of SG connected to a BTB converter with a rotor-side three-phase voltage source was verified in RTDS with CHIL setup, and the tracking performance of rotor-side controller is validated.

1 General Information of the User Project

The general information of the user project is shown as below.

User Project Title: Asynchronized Synchronous Motor based Shipboard Power System for All Electric Ship

User Project Acronym: ASM-based SPS for AES

Host Infrastructure: ICCS-NTUA

Start date – End date: 30/09/2018 – 26/10/2018

User Group Members:

1) Member 1 of the proposing user group: **Mr.Kai Ni**

Mr.Kai Ni is a Ph.D student of Dr.Yihua Hu in Department of Electrical Engineering & Electronics at University of Liverpool. His research interests include operation and control of asynchronized synchronous machine, power electronic converters, and power management. He is involved in a Ph.D project of CSols to reduce the carbon footprint in global laboratories.

In the proposed project he will set up the RTDS model of the proposed system, tune the control parameters and implement the control algorithms in CHIL setup.

2) Member 2 of the proposing user group: **Ms.Lujia Xie**

Ms.Lujia Xie is a Ph.D student of Dr.Yihua Hu in Department of Electrical Engineering & Electronics at University of Liverpool. Her research interests include motor design and optimization, magnetic field analysis and calculation, motor modelling and simulation, etc.

In the proposed project she will mainly focus on the motor analysis, modeling and simulation for the machines used in the proposed system.

2 Research Motivation

The concept of AES emerges to realize extensive electrification for modern ships, which reduces fuel consumption and increases the on-board power utilization rate. The normal operation of a commonly used fully decoupled SPS depends on power electronic devices, which are fragile and easy to break down. By applying the proposed partially power decoupled ASM-based SPS, the system robustness to power converter faults is increased and it becomes easier to isolate the faults.

2.1 Objectives

1. Set up the simulation model of an islanded microgrid based on a SG and an ASM.

2. Balance the power between the generator and load sides of the system under load variations.

3. Validate the normal system operation in the simulation environment.

4. Verify the control strategies for BTB converter in the CHIL setup, with the power hardware components simulated in RTDS.

2.2 Scope

During the stay in ICCS-NTUA, the user group aims to set up the models in RTDS software for the following power circuits: 1) an SG supplying a three-phase power rectifier; 2) a grid-connected three-phase power converter with DC voltage supply; 3) an SG connected to a BTB converter with the rotor of ASM simulated as a three-phase voltage source.

The implementation of the SG connected three-phase power rectifier aims to verify the DC bus voltage control scheme in the proposed SPS, and the current control performance in the grid-connected three-phase power converter with DC voltage supply is to be demonstrated by good tracking performance. Combining the two parts, the power circuit of SG connected with a BTB converter with the rotor of ASM simulated as a three-phase voltage source is established, and the aforementioned two targets will be achieved by tuning the controller parameters.

During the controller parameter tuning process, two switches are added in the “Runtime” interface of RTDS software to enable or disable the control of the grid-side converter (GSC) and rotor-side converter (RSC). The RSC is disabled at first, and the GSC is controlled to ensure the DC-bus voltage is stable and at the rated value. Afterwards, the control of RSC is activated to achieve the desirable rotor-side active and reactive power for ASM.

3 State-of-the-Art/State-of-Technology

The concept of AES has been put forward in recent years to meet the requirements of saving fuel consumption and increasing the on-board power utilization rate, and this concept has become a standard in the field of large cruise ships [1]. Thanks to the development of power electronics techniques, multiple energy sources, independent operation of individual power producers, and energy storage became available in AES. Following this trend, a number of research achievements were published in this field, in terms of power electronics topologies [2-16], system control and optimization algorithms [17-27], power management strategies [28-37], system stability and reliability studies [38-42].

Power electronic devices are widely used in AES, and they are of paramount significance to the reliable operation of SPS. In order to increase the system power level, efficiency, power density and reliability, various categories of voltage source converter (VSC) topologies were proposed, including multilevel converters [2-4], interleaved converters [5], multi-phase converters [6, 7], soft-switched converters [8], and power electronics building blocks (PEBBs) [9-10]. Among them, multilevel converter is the most popular one, and some typical multilevel topologies were illustrated in [11]. The modular multilevel converter (MMC) attracts the most attention since it is endowed with the advantages of high modularity, high scalability, and high efficiency [12-13]. In [14], a scalable metamodel was illustrated for compatible MMCs. Besides, the topology, modelling, and control of isolated modular multilevel DC-DC converters were investigated in [15-16].

Regarding the control and optimization schemes for AES, except the conventional proportional-integral (PI) and model predictive control (MPC) strategies, a number of computational intelligence (CI) methods were used. In [17-20], the particle swarm optimization (PSO) algorithm was investigated. In addition, the fuzzy set theory [21], neural network [22], and genetic algorithm [23-26] were employed for optimization of different control purposes. Furthermore, the hierarchical control technology in smart grids and DC microgrids were employed to control SPS [27]. In this control scheme, three control levels were defined, which are the primary, secondary and tertiary control levels, aiming at the power electronics interface control, grid power quality, and power exchange management, respectively.

A substantial number of investigations were also carried out in the power management strategies for AES. In [28], the optimal operation of SPS was studied to achieve the targets of reducing fuel consumption and greenhouse gas (GHG) emissions. Meanwhile, the corresponding technical and operational constraints were obeyed. Besides, for the optimal demand-side power management method proposed in [29], dynamic programming was employed with the ship load forecasting assumed to be available, and the energy storage system and investment capital were not required. Moreover, a dynamic positioning system was investigated in [30] as the dynamic energy storage. Furthermore, a novel integrated security-constrained power management (ISCPM) method was proposed in [31], and it was formulated as a multi-objective optimization problem.

In order to save the on-board space and weight, flexibly arrange the equipment, and omit reactive power compensation components, a novel medium voltage direct current (MVDC) integrated power system (IPS) was proposed [32]. In [33], the power flow studies in shipboard MVDC distribution systems were conducted for system planning. The multi-agent system-based (MAS-based) real-time load management technique was employed to determine the switch status of the loads in DC zones and satisfy the real-time system operating constraints simultaneously [34]. In [35], a fuzzy logic based energy storage management (ESM) system was proposed for power regulation in MVDC IPS. In addition, an EMS controlled by PSO strategy was investigated in [36]. Moreover, an IPS consisting of fuel cells, batteries, photovoltaic (PV) panels, and diesel generators was proposed and modelled for AES in [37]. However, with the application of MVDC architecture for AES, new fault protection strategies should be developed, including fault detection, protection device coordination, system reconfiguration, and fault isolation [38]. In [39], the problem of constant power load (CPL) instability is focused on, and a linearization via state feedback based control method was proposed to solve it.

Besides, the first medium-voltage impedance measurement unit (IMU) was designed to assess the SPS stability in [40]. On top of that, an active impedance estimation scheme was proposed in [41] to accurately locate the fault in a zonal DC SPS. Furthermore, the opinion of carrying out the diagnostic knowledge management from the earliest stages of ship design was developed in [42].

4 Executed Tests and Experiments

In this project, the user group built up the models for the power circuits of SG with its excitation system and governor, ASM, and BTB converter in the RTDS software. The control strategies for BTB converter are implemented in Simulink on a target PC with CHIL setup [43][44]. The PLL, Park and Inverse Park Transformation blocks, and the calculations of active and reactive power are carried out in the RTDS software. The measurements used for implementing control strategies are input into the CHIL setup by digital/analogue (D/A) interface, and the control signals for the BTB converter are output from the CHIL setup by analogue/digital (A/D) interface.

4.1 Test Plan

The test is generally divided into three parts:

1) The control of SG connected with a GSC supplying the DC-bus capacitor is to be verified to obtain a stable DC-bus voltage and sinusoidal three-phase grid-side AC currents.

2) The control of RSC connected to a three-phase voltage source is to be verified to achieve good tracking performances for the dq currents and active/reactive power.

3) The SG connected with BTB converter that supplied by a three-phase voltage source is to be controlled to achieve all the targets described in 1) and 2).

4.2 Standards, Procedures, and Methodology

The procedures of the RTDS simulations with CHIL setup are shown below.

1) Establish the power circuit of a three-phase AC voltage source feeding a GSC to charge the DC-bus capacitors in RTDS software.

2) Set up the voltage source, Park Transformation, Inverse Park Transformation, power calculation, PLL, D/A and A/D blocks in RTDS software for the system in 1).

3) Set up the DC-bus voltage and grid current control blocks in Simulink with Triphase input/output blocks.

4) Adjust the scaling of the variables to be used in the D/A and A/D blocks in RTDS software to make sure the readings of measurements in RTDS software and Simulink are the same.

5) Compile the draft in RTDS software, and build up and activate the control model in Simulink by using an external target PC.

6) Run the simulation and tune the PI control parameters to obtain acceptable control performance for the system.

7) Display the plots in the “Runtime” interface of RTDS software.

8) Implement a step change in the reference value of current during the simulation process, and then save the obtained waveforms.

9) Establish the power circuit of a SG with Type 1 exciter and governor that feeds a GSC to charge the DC-bus capacitors in RTDS software.

10) Set up the voltage source, Park Transformation, Inverse Park Transformation, power calculation, PLL, D/A and A/D blocks in RTDS software for the system in 9).

11) Repeat Steps 3) to 8) for the system in 9).

12) Establish the power circuit of a RSC with DC voltage supply that connects to a three-phase power grid in RTDS software.

13) Set up the voltage source, Park Transformation, Inverse Park Transformation, power calculation, PLL, D/A and A/D blocks in RTDS software for the system in 12).

14) Repeat Steps 3) to 8) for the system in 12).

15) Establish the power circuit of a SG with Type 1 exciter and governor that feeds a BTB that connects to a three-phase power grid in RTDS software.

16) Set up the voltage source, Park Transformation, Inverse Park Transformation, power calculation, PLL, D/A and A/D blocks in RTDS software for the system in 15).

17) Repeat Steps 3) to 8) for the system in 15).

4.3 Test Set-up(s)

4.3.1 Implementation Details

In the ASM-based SPS in this project, the DC-bus voltage should be kept at a steady value to ensure a stable DC voltage supply for the rotor side of ASM is stable. In addition, the three-phase currents from the SG should be in almost sinusoidal waveforms to ensure the quality of power generation is good enough. A high input power factor is also to be achieved. Therefore, the main tasks of the GSC connected to the SG are maintaining a steady DC-bus voltage for the DC-bus capacitor, sinusoidal three-phase input current waveforms, and high power factor.

On the other hand, the RSC is used to control the operation of ASM, which is connected to the rotor of ASM. The back electromagnetic force (EMF) for the stator of ASM is represented by a three-phase voltage source with the slip frequency. The case of constant rotor speed is taken into consideration in this study, and the tracking performance of the rotor currents and power will be verified in the tests. The illustrations of the tests carried out during the stay are presented as follows.

1) Firstly, a three-phase voltage source with the same rated voltage and frequency as those of the SG is applied to feed a GSC. In this case, the influence of excitation control for the SG is ignored. The small time-step circuit model of the three-phase voltage source connected to a GSC with DC-bus capacitors in RTDS is displayed in Figure 1.

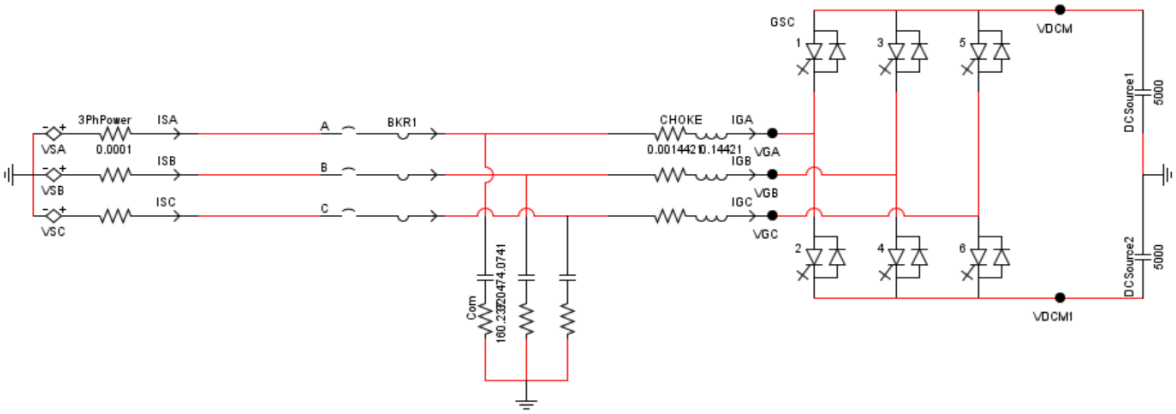

Figure 1: GSC fed by a three-phase voltage source

A three-phase voltage source with the same voltage rating and frequency as those of the SG is applied to provide power supply for the GSC. A three-phase RC compensator is connected with the GSC in parallel to compensate the reactive power in the circuit. In the DC-bus, two capacitors are used, with the ground connected at the midpoint.

2) Secondly, the SG with IEEE Type 1 excitation system and governor is used to produce three-phase voltages for the GSC. The excitation process is directly realized in RTDS software, thus only the control strategy for the GSC needs to be implemented in Simulink by using the CHIL setup. The small time-step power circuit of this system is displayed in Figure 2.

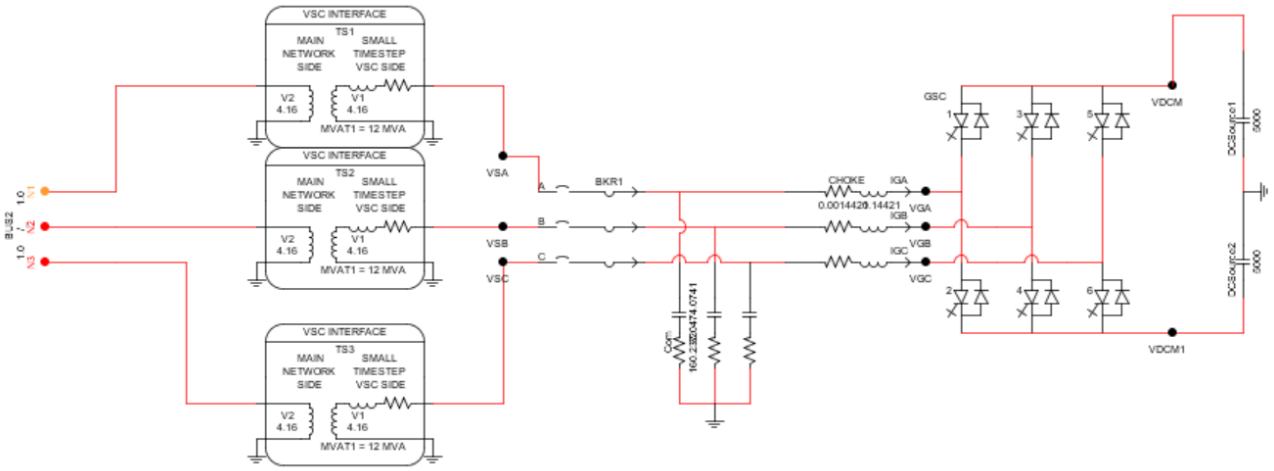

Figure 2: Small time-step power circuit of SG connected to GSC

The normal operation of SG can be verified first by opening the three-phase circuit breaker. Then the circuit breaker is closed to connect the SG to the GSC to verify the operation of the whole circuit. The three single-phase transformers are applied to connect the small time-step part of the power circuit to the large time-step part, which is displayed in Figure 3.

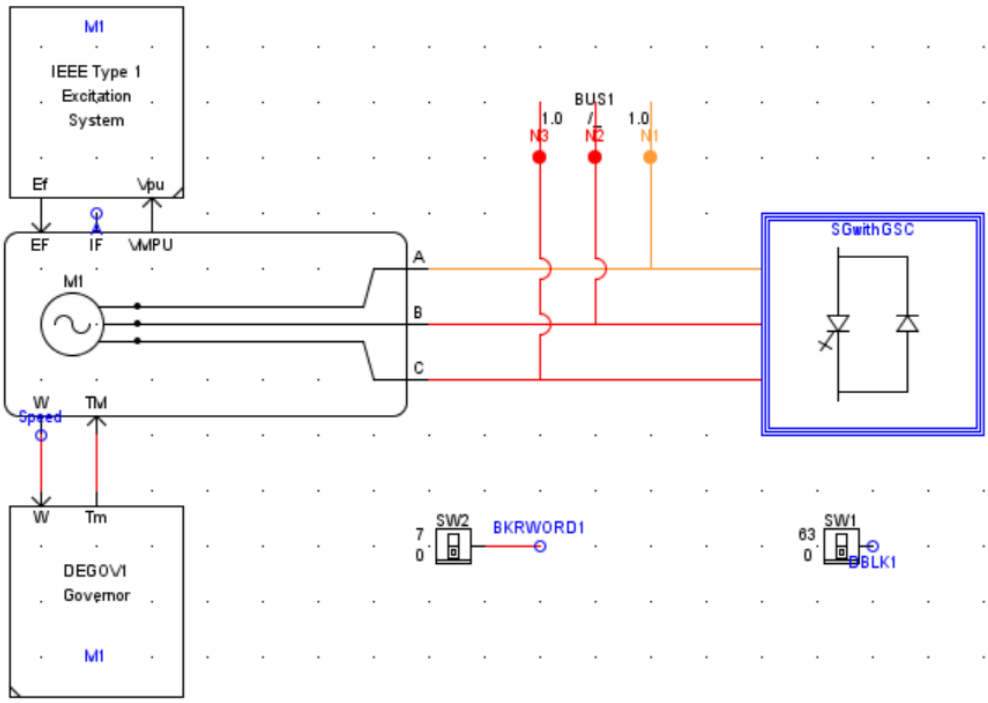

Figure 3: SG with IEEE Type 1 excitation system and governor to connect to GSC

The output three-phase voltages of the SG are controlled by using the IEEE Type 1 excitation system, and the governor is applied to input the mechanical torque to the SG.

3) Thirdly, the power circuit of RSC is established in RTDS software, with constant DC voltage source and a three-phase power grid used to stimulate the three-phase voltages supplied from the stator to the rotor of ASM. The power circuit of RSC connected to a three-phase power grid is shown in Figure 4.

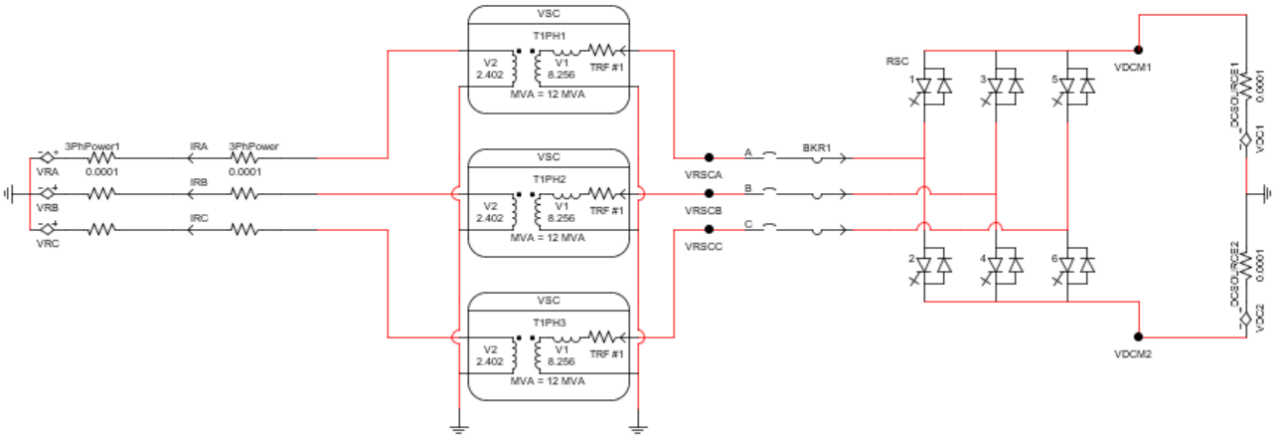

Figure 4: Small time-step power circuit of RSC connected with a power grid

4) Finally, the two power circuits in 2) and 3) are combined to form the circuit of an SG supplying the BTB converter that is connected to a three-phase power grid. The power circuit in small time-step modelling is displayed in Figure 5.

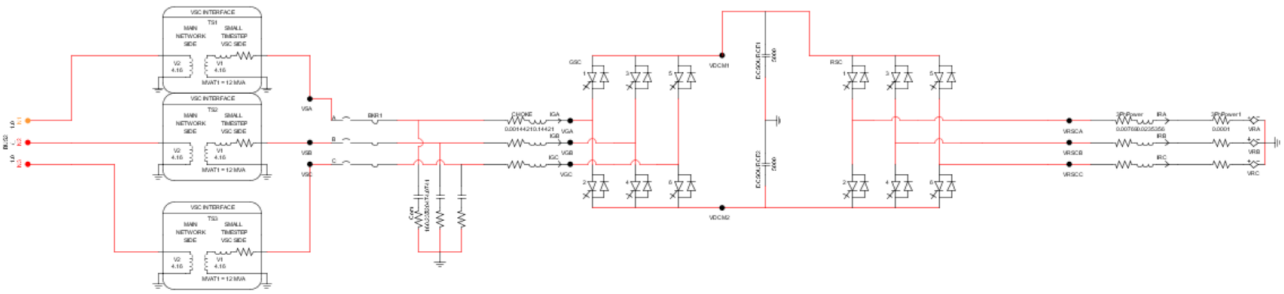

Figure 5: Small time-step power circuit of SG connected to BTB converter with grid connection

The normal operation of SG can be verified first by opening the three-phase circuit breaker. Then the circuit breaker is closed to connect the SG to the BTB. The GSC is controlled first with the RSC uncontrolled to see if the rectifying procedure is implemented correctly to maintain a steady DC-bus voltage for the rotor side. Then the RSC control is activated to verify the normal operation of the whole power circuit. The three single-phase transformers are applied to connect the small time-step part of the power circuit to the large time-step part, which is displayed in Figure 6.

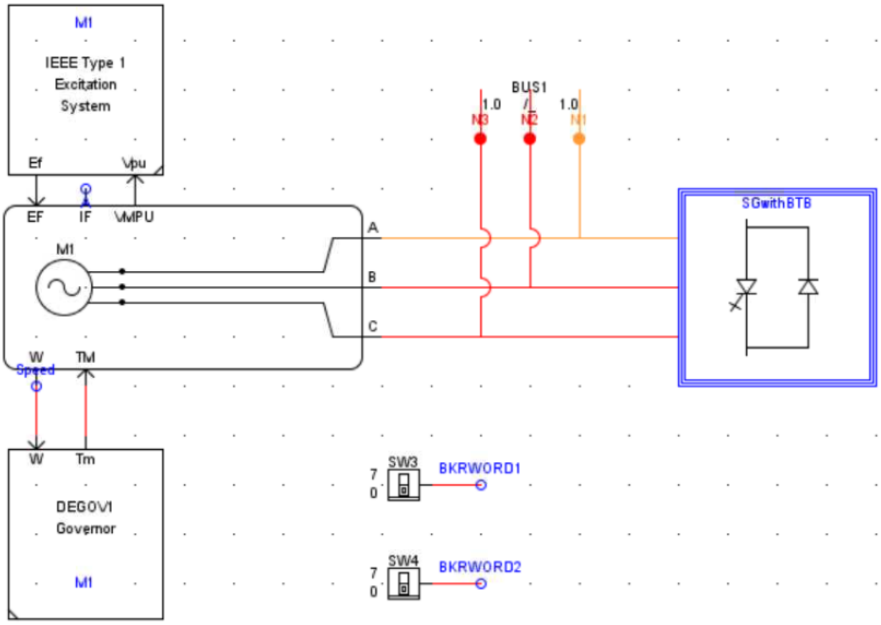

Figure 6: SG with IEEE Type 1 excitation system and governor to connect to BTB converter

4.3.2 Equipment and Communications Involved

In the project, the equipment used are a PC, RTDS, and CHIL setup. The power circuits mentioned in the previous section and the signal processing blocks are established in RTDS software, while the control block diagrams for the GSC and RSC are built up in Simulink and run in CHIL setup on a target PC. The variables to be used for controlling the BTB converter are output from RTDS software to the target PC, and at the same time the control signals for the power switches in the BTB converter in the power circuit are input to RTDS software from the target PC. The setup of the simulation platform is shown in Figure 7.

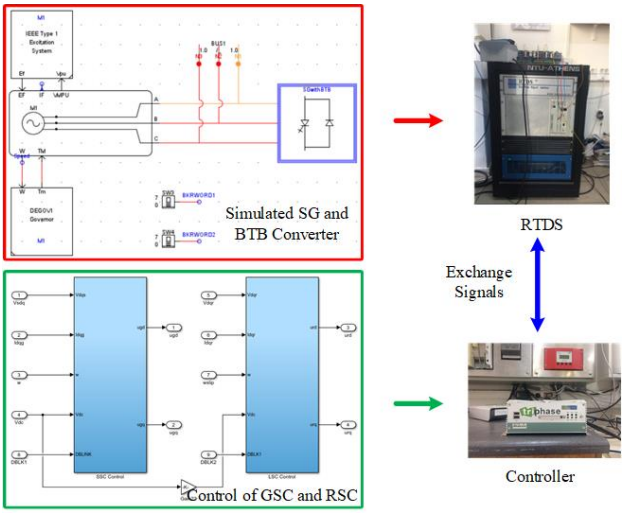

Figure 7: Real-time simulation platform setup

4.3.3 Control Strategy

In order to control the circuit of three-phase voltage source supplying a GSC, the signal processing diagram of the system is set up as shown in Figure 8, where the magnitude and frequency of three-phase voltage source V_{SABC} are defined at the right bottom corner of the figure. At the left bottom corner, a PLL is applied to derive the grid frequency and angle provided by the three-phase voltage source. The input dq voltages and currents of GSC are achieved by using Park Transformation, and

the input active and reactive power are calculated. The output variables to the target PC are the dq voltages and currents at the AC side of GSC, the grid angular frequency, DC-bus voltage, and the switching function of GSC. The control signals in the dq frame are the outputs from the target PC. They are converted back to abc coordinate system for controlling the power switches in GSC.

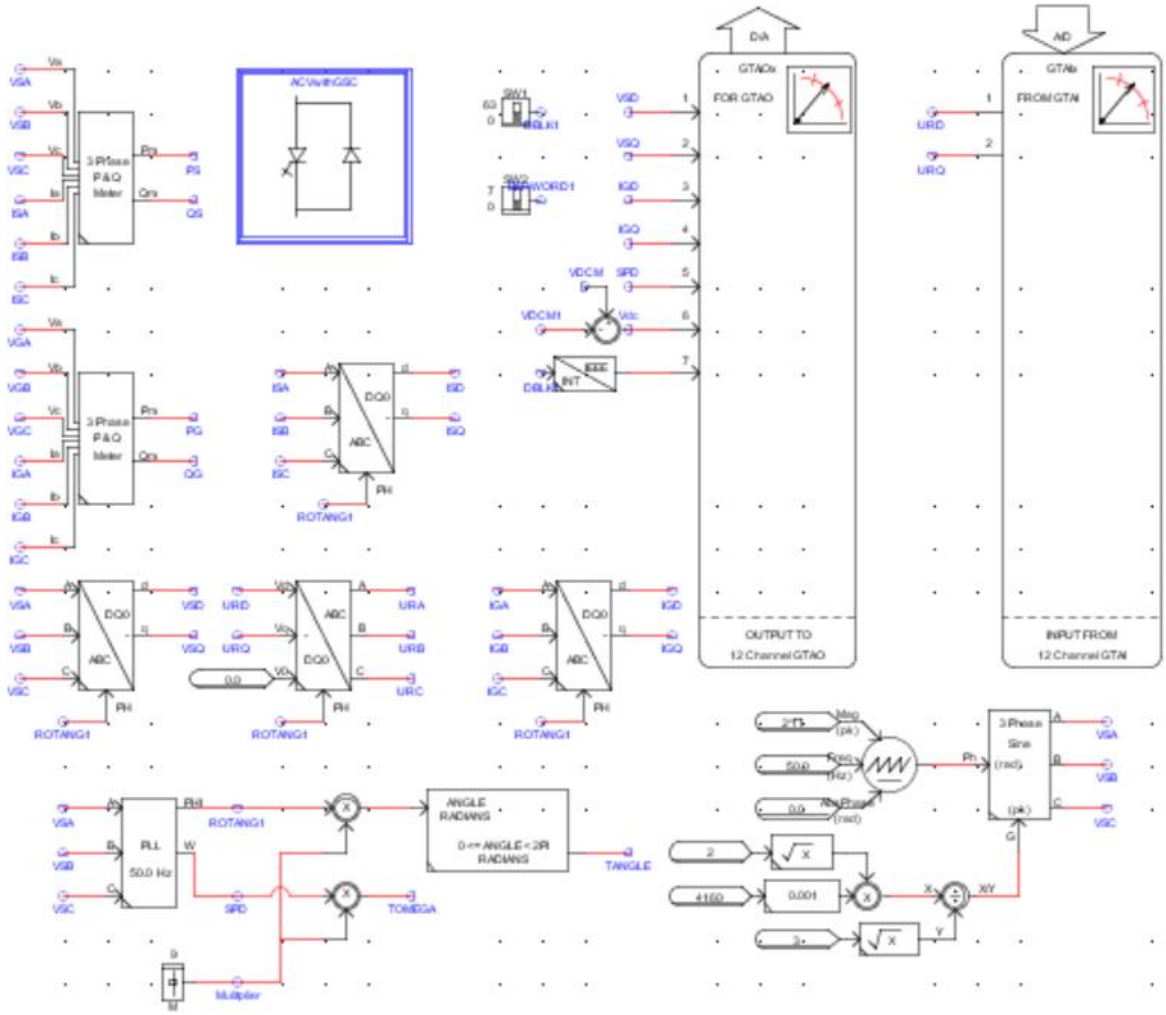

Figure 8: Signal processing diagram *of the GSC connected three-phase voltage source*

The signal processing diagram for GSC in Simulink is displayed in Figure 9.

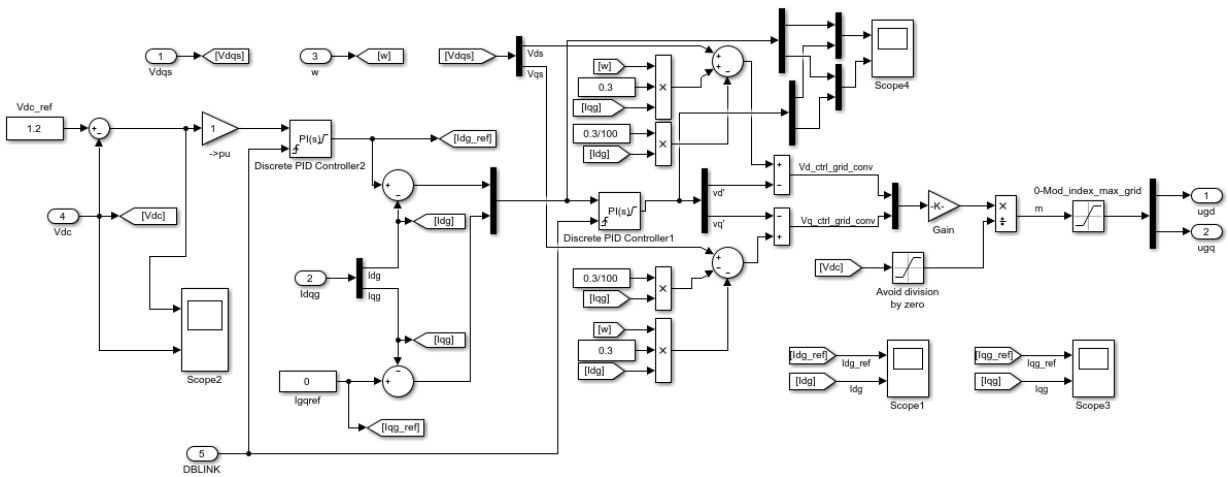

Figure 9: Control block diagram for GSC

The d-axis current reference value is derived from the DC-bus voltage control loop, and the q-axis current reference is directly set by the user. The switching signal “DBLINK” for the GSC is injected to the PI controllers for the voltage and current control loops. Once the control of GSC is enabled, the PI controller parameters will be updated.

After the SG is used in the power circuit in RTDS software, the excitation control is completed by the IEEE Type 1 excitation system, and the governor is used to regulate the speed of SG. The other signal processing blocks and the control blocks of GSC remain the same as those in the previous case. The signal processing diagram of GSC connected with SG is displayed in Figure 10.

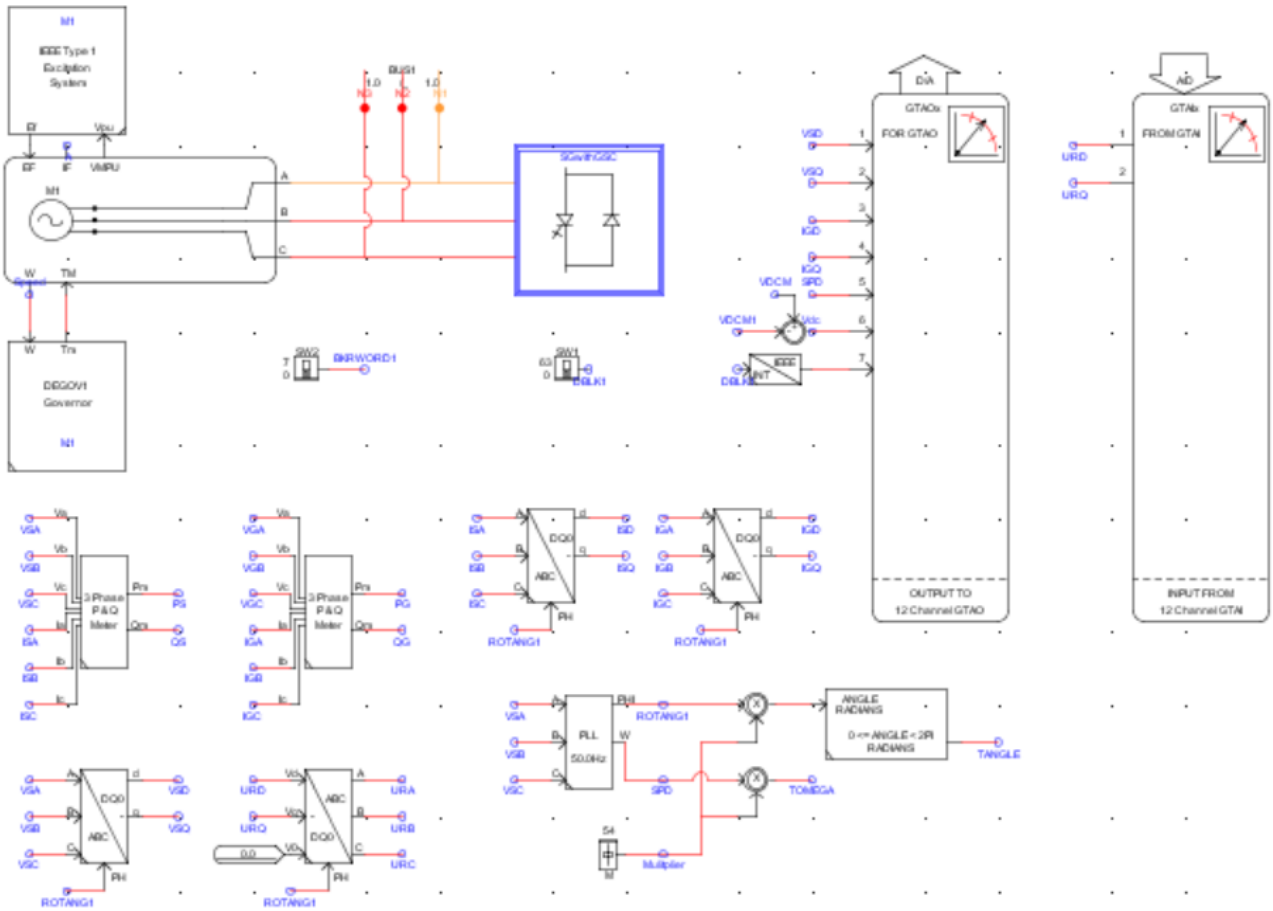

Figure 10: Signal processing diagram of GSC connected with SG

For the rotor side of the system, the signal processing diagram is shown in Figure 11 for controlling the RSC connected to a power grid, whose frequency is equal to the slip times the nominal grid frequency. The magnitudes of the three-phase voltages and DC-bus voltages are defined manually.

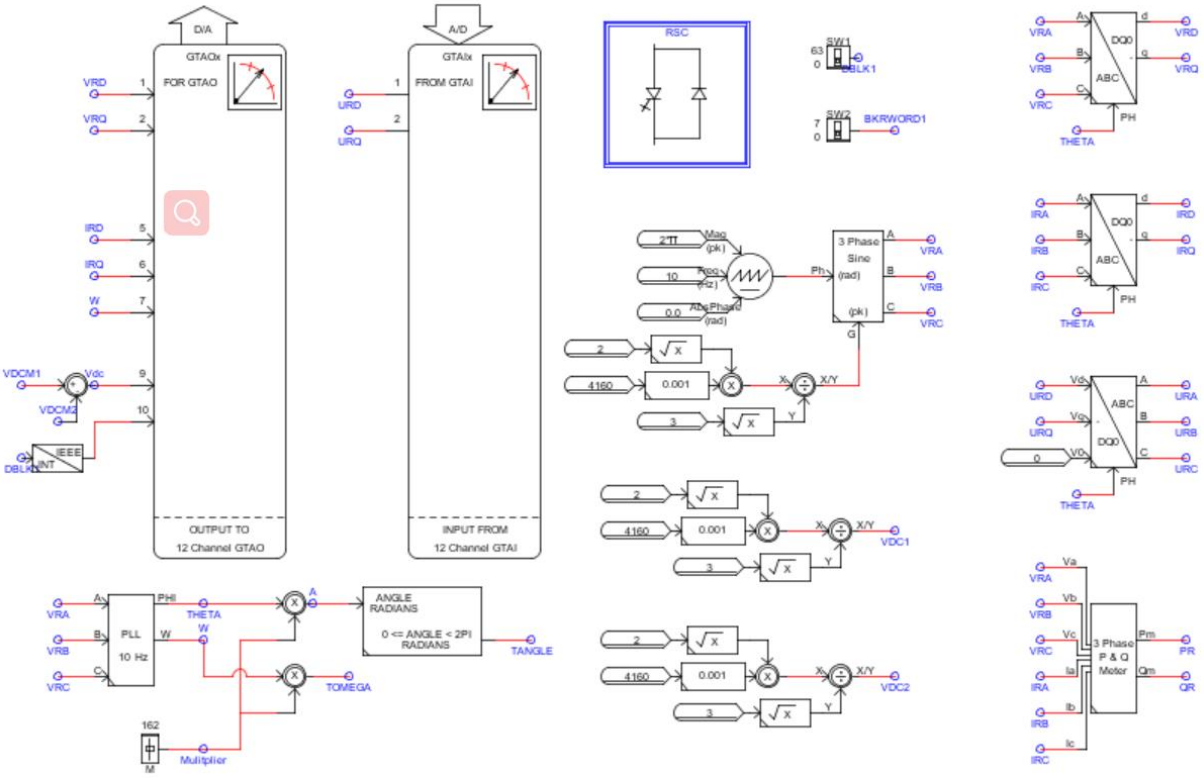

Figure 11: Signal processing diagram of RSC connected to a power grid

The control block diagram in Simulink for the RSC connected to a power grid are shown in Figure 12.

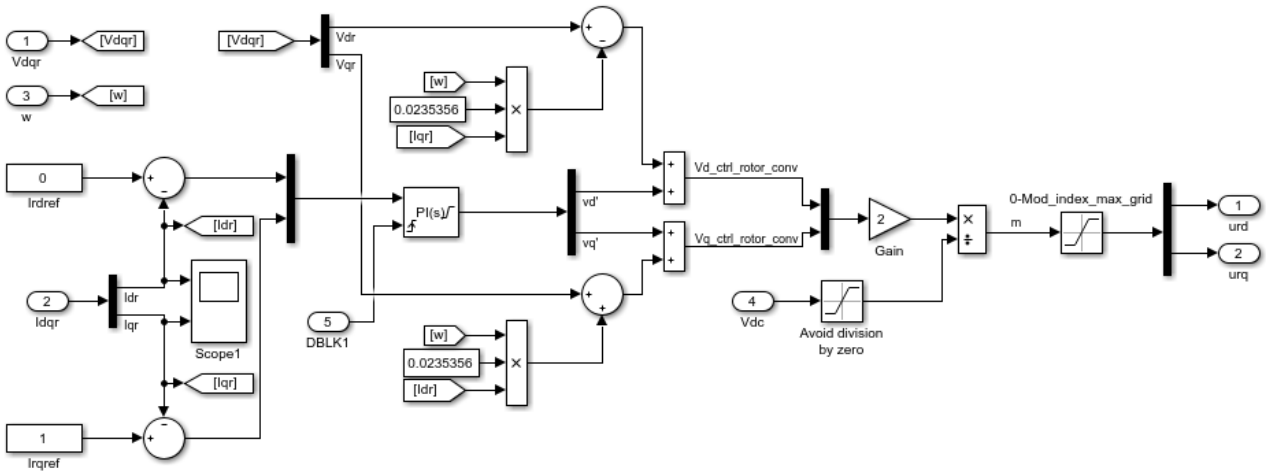

Figure 12: Control block diagram of RSC connected to a power grid

The slip is a fixed value in the test, and the dq rotor current reference values are determined by the user. The tracking performance of RSC will then be verified.

After the control performances of GSC and RSC are both verified, the circuit of an SG connected with BTB converter is established to verify the performance of the whole circuit. The signal processing diagram of the whole circuit to be verified is displayed in Figure 13.

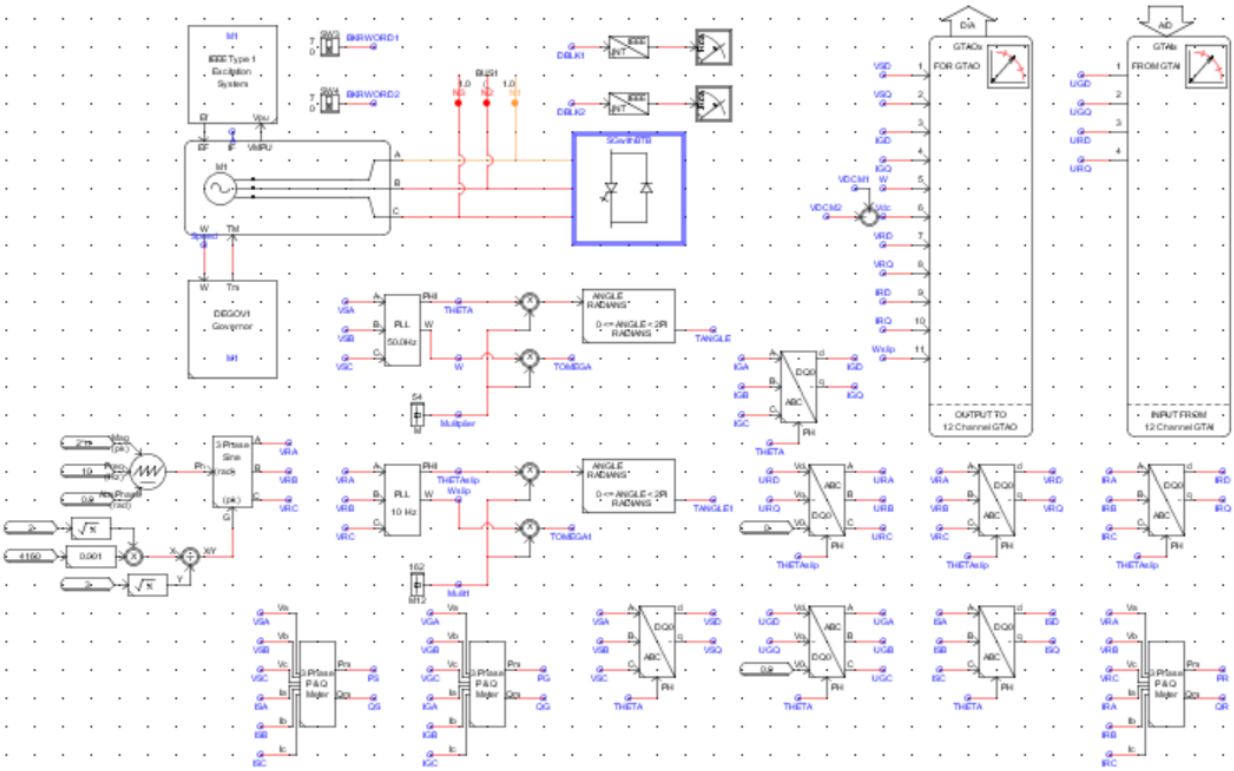

Figure 13: Signal processing diagram of SG connected with BTB converter

The circuit of SG connected with a GSC and that of RSC connected to a power grid are combined together to form the whole circuit for the RTDS test in CHIL setup. The GSC and RSC are separately controlled by the control signals from the target PC, which are *UGD*, *UGQ*, *URD* and *URQ* in Figure 13. There are 13 outputs from RTDS software in total, which are the dq stator voltages (*VSD* and *VSQ*), dq currents for GSC (*IGD* and *IGQ*), synchronous grid angular frequency (*W*), DC-bus voltage (*Vdc*), dq rotor voltages (*VRD* and *VRQ*), dq rotor currents (*IRD* and *IRQ*), slip angular frequency (*Wslip*), switching commands for GSC and RSC (*DBLK*1 and *DBLK*2).

The control blocks for GSC and RSC are combined together to control the BTB converter. The control blocks are established by using two subsystems, which are shown in Figure 14.

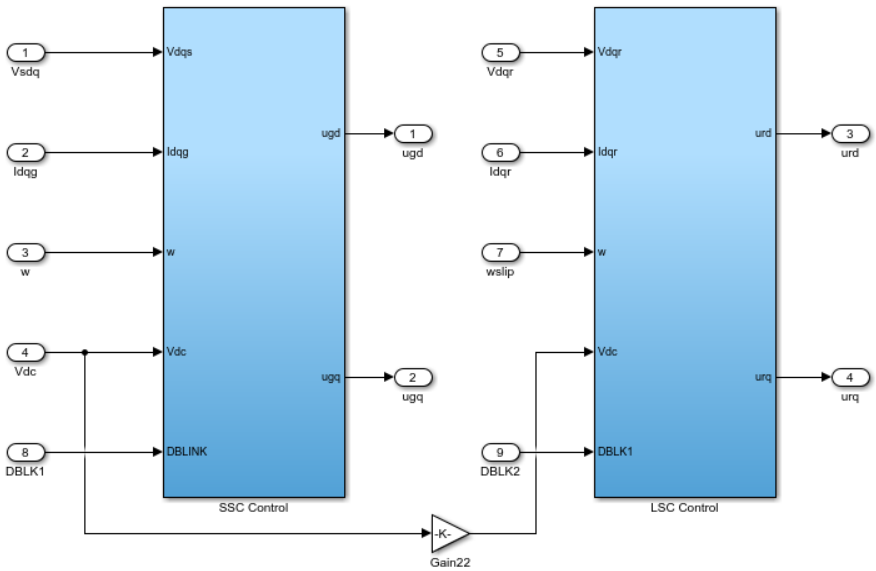

Figure 14: Control blocks for BTB converter

4.3.4 Monitoring Aspects

After the power circuits discussed in previous sections are compiled and run in RTDS successfully, the control strategies in Simulink are uploaded to CHIL setup and implemented. Then, the controller parameters are tuned to obtain the desirable results. The plots of the key measurements are added to the “Runtime” interface in RTDS software. For example, the DC-bus voltage should be maintained at a nearly constant value. By refreshing the plots or monitoring the signal in Simulink by using a scope, the variations in DC-bus voltage can be clearly observed. Since the simulation is in real time, the tracking performance of the signal will vary instantly with the modifications in the parameters of controllers. When the circuit parameters are modified in RTDS software, the power circuit needs to be complied again to update the changes. For the other measurements, the monitoring processes are the same.

4.4 Data Management and Processing

The data used for the power circuits in RTDS tests are the same as those used in the Simulink model of ASM-based SPS, which has been established and verified before the stay in NTUA. After running the RTDS model, the corresponding plots are displayed in the “Runtime” interface, and they are saved with the data stored in the format of m files in Matlab. The data can be extracted for drawing the plots with specified scale ranges for the x and y axes.

5 Results and Conclusions

5.1 Parameter Setup

The simulation studies in RTDS are carried out by using the parameters shown in Tables 1 to 3 for the proposed power system.

Table 1: Parameters of synchronous generator

Description	Value	Unit
Rated apparent power	36	MVA
Rated RMS line-to-line voltage	4.16	kV
Base angular frequency	50	Hz
Inertia constant	3.5	MWs/MVA
Synchronous Mechanical Damping	0	/
Stator leakage reactance	0.075	pu
d-axis unsaturated reactance	1.321	pu
d-axis unsaturated transient reactance	0.1685	pu
d-axis unsaturated sub-transient reactance	0.105	pu
q-axis unsaturated reactance	1.173	pu
q-axis unsaturated sub-transient reactance	0.09	pu
Stator resistance	0.036	pu
d-axis unsaturated transient open-circuit time constant	6.5	Second
d-axis unsaturated sub-transient open-circuit time constant	0.0241	Second
q-axis unsaturated sub-transient open-circuit time constant	0.0464	Second

Table 2: Parameters of IEEE Type1 excitation system

Description	Value	Unit
Voltage transducer time constant	0.02	Second
Voltage regulator gain	300	/
Voltage regulator time constant	0.001	Second
Maximum control element output	2	pu
Minimum control element output	-2	pu
Exciter field resistance line slope margin	1	pu
Exciter field time constant	0.0001	Second
Rate feedback gain	0.0001	pu
Rate feedback time constant	0.1	Second

Table 3: Power circuit parameters

Description	Value	Unit
Rated apparent power	36	MVA
Rated grid line-to-line voltage	4.16	kV
Rated rotor line-to-line voltage	4.16	kV
Grid-side base angular frequency	50	Hz
Rotor-side base angular frequency	10	Hz
Resistance of reactive power compensator	160.237	Ohms
Capacitance of reactive power compensator	320474.0741	MicroF
Resistance of grid-side filter	0.0014421	Ohms
Inductance of grid-side filter	0.14421	Henries
DC-bus capacitance	10000	MicroF
Rotor resistance	0.00769	Ohms
Rotor inductance	0.0235356	Henries
Rate feedback gain	0.0001	pu
Rate feedback time constant	0.1	Second
Valve switching voltage magnitude	4	kV
Valve switching current magnitude	4	kA

Valve RLD damping factor	0.7	pu

In order to appropriately control the BTB power converters in RTDS, the measurements in CHIL should correspond to those in RTDS (control signals are in either pu or SI units). The scaling for the outputs from RTDS software is displayed in Table 4.

Table 4: Scaling for the output signals from RTDS software

Description	Value
Peak value of dq grid voltages for 5 Volts D/A out	16.983
Peak value of dq grid currents for 5 Volts D/A out	24.982
Peak value of synchronous angular speed for 5 Volts D/A out	1570.796327
Peak value of DC-bus voltage for 5 Volts D/A out	33.966
Peak value of dq rotor voltages for 5 Volts D/A out	16.983
Peak value of dq rotor currents for 5 Volts D/A out	160.237
Peak value of slip angular speed for 5 Volts D/A out	1570.796327
Peak value of power converter control signal for 5 Volts D/A out	315

5.2 Simulation Results for Three-Phase Voltage Source Feeding GSC

At the first stage, the influence of the SG parameters is not taken into account, and the SG is regarded as a stable three-phase grid voltage source that supplies power to the system. The control of GSC is enabled at 2s in the simulation, and the simulation results are displayed in Figures 15 & 16.

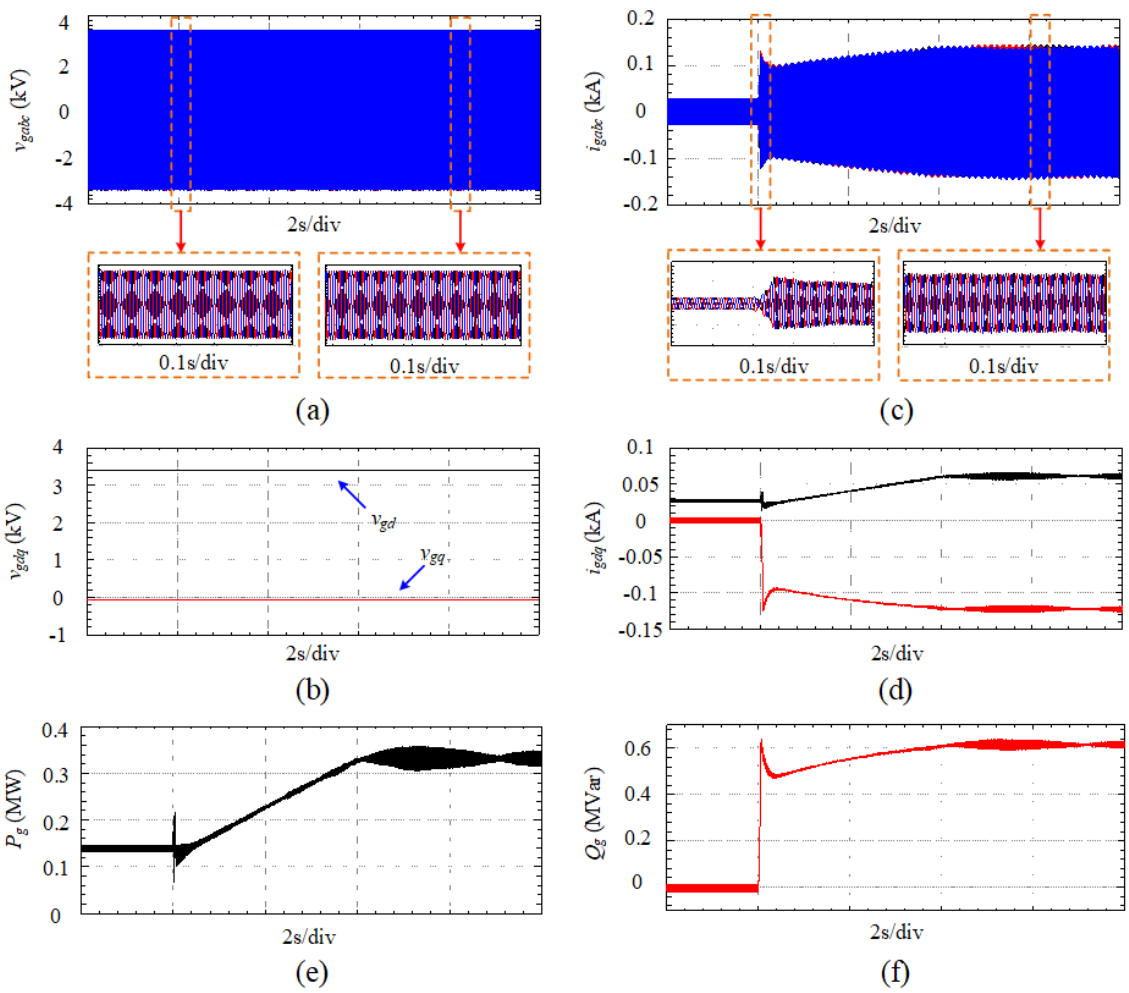

Figure 15: Simulation results for the variables of three-phase voltage source by turning on the GSC control at

2s (a) three-phase grid voltages; (b) dq grid voltages; (c) three-phase grid currents; (d) dq grid currents; (e) grid active power; (f) grid reactive power

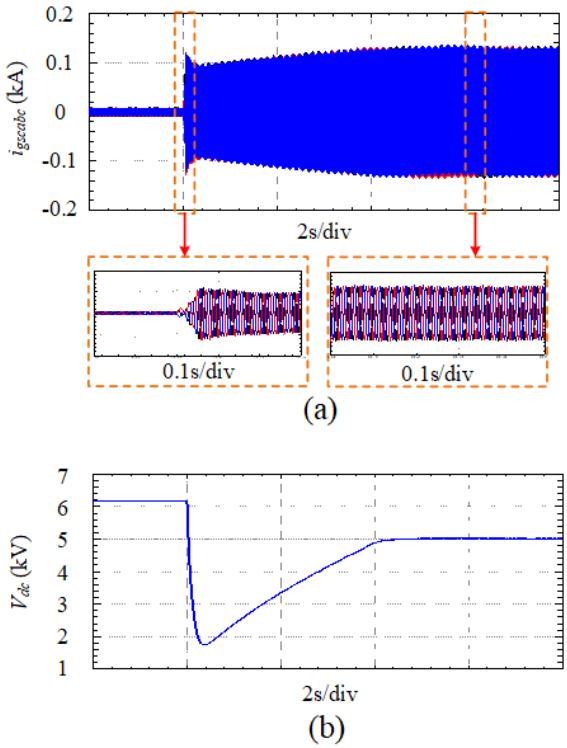

Figure 16: Simulation results for the variables of GSC with a three-phase voltage supply by turning on the GSC control at 2s (a) three-phase GSC currents; (b) DC-bus voltage

It can be seen from Figure 15 that the grid three-phase voltages are stable during the whole simulation process, and the decoupling between the dq grid voltages v_{gd} and v_{gq} is perfectly completed. After turning on the control of GSC, the magnitude of three-phase grid currents keeps increasing until it reaches 0.15kA, and the waveforms are almost sinusoidal from the enlarged plots shown in Figure 15(c). In addition, the active and reactive power take about 4s to reach the new steady values.

The performance of GSC is displayed in Figure 16. The three-phase GSC currents have the similar performance as that of the three-phase grid currents, except that the magnitude is a little bit smaller. It can be seen from Figure 16(b) that the DC-bus voltage drops to a value below 2kV after turning on the control of GSC, and it raises up to approximately 5kV at 6s to achieve the stable operation.

5.3 Simulation Results for SG Connected with GSC

Then, an SG is directly connected to the GSC to provide power. The GSC control was turned on at 2s to see the control effects, which are displayed in Figures 17 & 18.

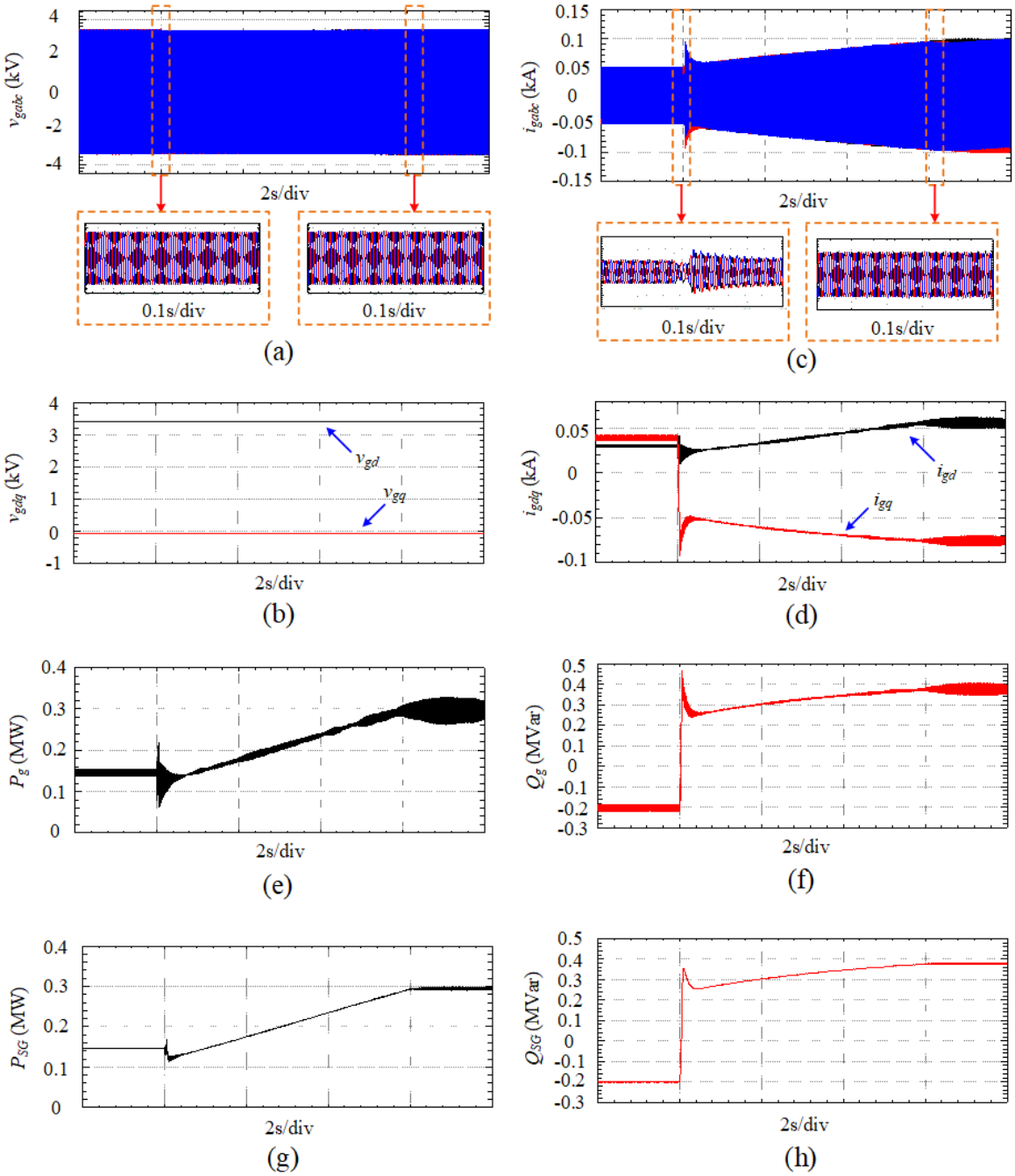

Figure 17: Simulation results for the SG variables by turning on the GSC control at 2s (a) three-phase grid voltages; (b) dq grid voltages; (c) three-phase grid currents; (d) dq grid currents; (e) grid active power; (f) grid reactive power; (g) SG output active power; (h) SG output reactive power

From Figure 17, it can be seen that the three-phase voltages supplied by SG are stable during the whole process of simulation, and the dq grid voltages are completely decoupled. There are some ripples in the three-phase grid currents at the point of turning on the GSC control, and it takes around 6s to achieve the steady operating state. In addition, the sinusoidal current waveforms are obtained as can be seen in Figure 17(c). Comparing the power generated to the system (Figure 17(e) & (f)) with that generated directly from SG (Figure 17(g) & (h)), there are some noises owing to the use of VSC interfaces between the SG and the power circuit of the rest part of the system.

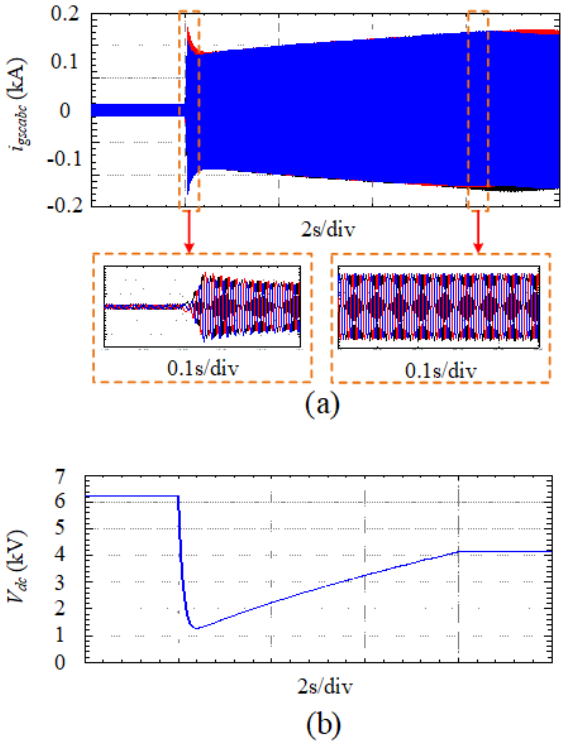

Figure 18: Simulation results for the variables of GSC with an SG power supply by turning on the GSC control at 2s (a) three-phase GSC currents; (b) DC-bus voltage

From Figure 18(a), the three-phase GSC currents achieve the magnitude of around 0.17kA after 8s, and almost sinusoidal current waveforms are obtained. The DC-bus voltage drops from the nominal value to a value above 1kV, and then moderately increases back to over 4kV.

In order to investigate the Automatic Voltage Regulator impact on the overall system, the voltage set point was increased from 1 to 1.2. The simulation results in this case are displayed in Figures 19 & 20.

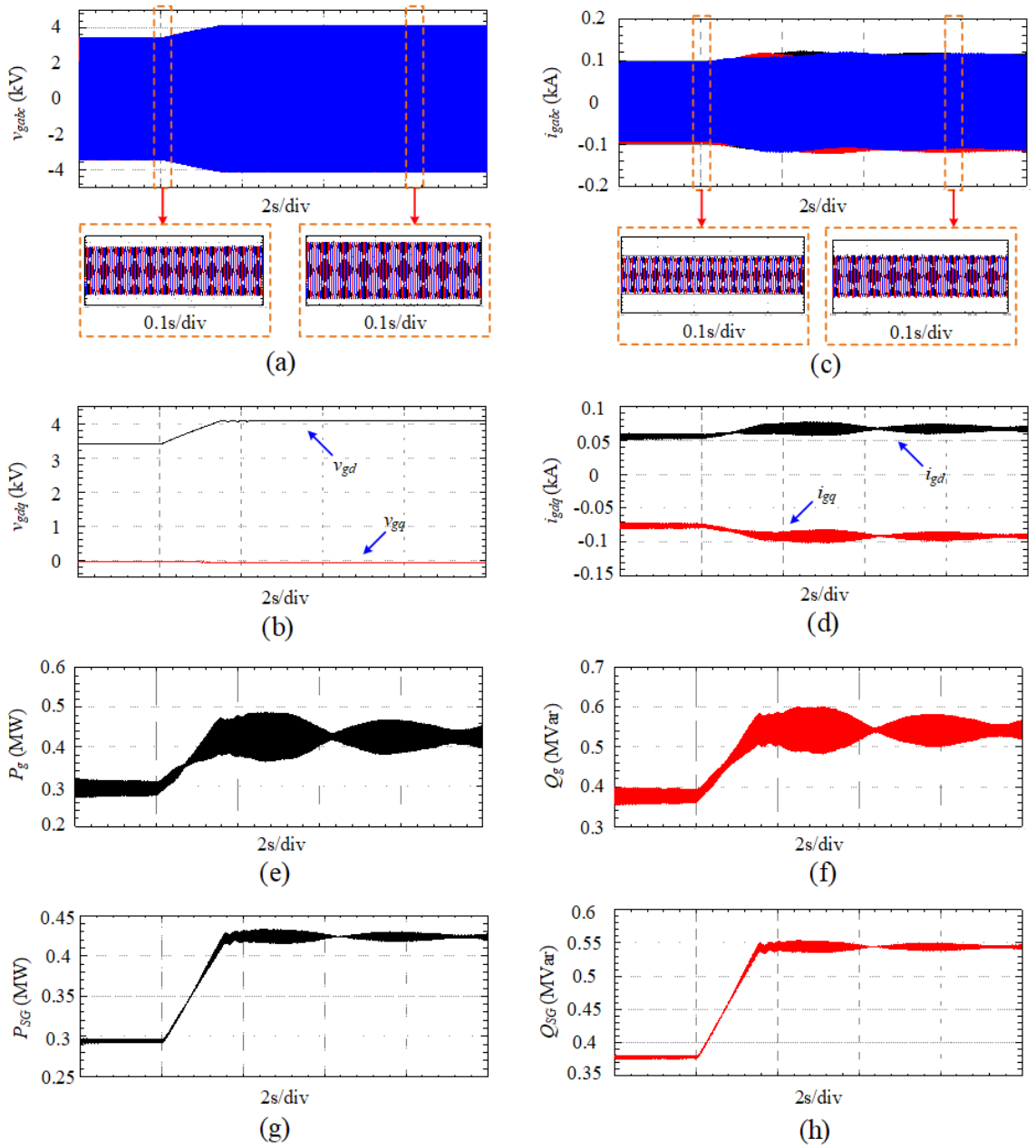

Figure 19: Simulation results for the SG variables by changing the exciter gain from 1 to 1.2 at 2s (a) three-phase grid voltages; (b) dq grid voltages; (c) three-phase grid currents; (d) dq grid currents; (e) grid active power; (f) grid reactive power; (g) SG output active power; (h) SG output reactive power

From Figure 19, it can be seen that the magnitudes of the three-phase grid voltages and current both increase, resulting from the increase in the active and reactive power from the GSC.

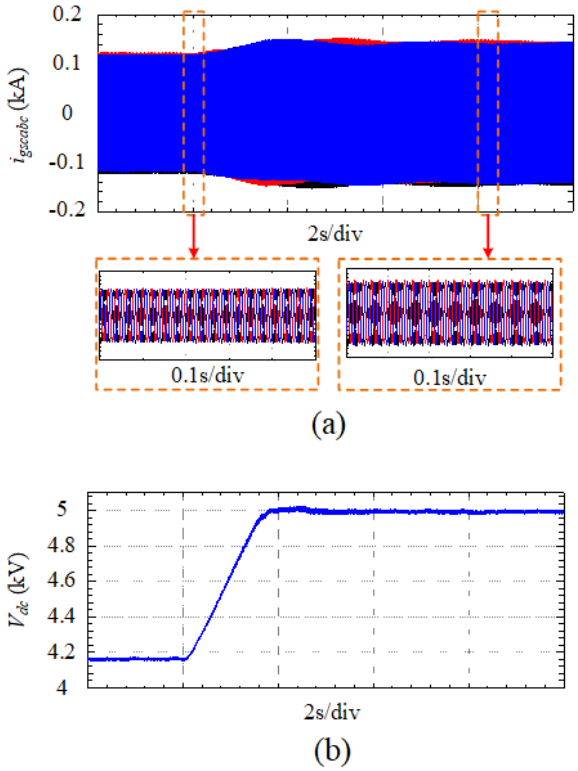

Figure 20: Simulation results for the variables of GSC with an SG power supply by changing the exciter gain from 1 to 1.2 at 2s (a) three-phase GSC currents; (b) DC-bus voltage

From Figure 20, it can be seen that the three-phase GSC currents still maintain almost sinusoidal waveforms after increasing the exciter gain, and some fluctuations can be observed. The DC-bus voltage boosted from 4.16kV to around 5kV.

The cases shown in Figures 17 - 20 are carried out by forcing the SG to operate at the synchronous speed (lock mode). For the sake of simulating a more practical case where the rotor angular speed of SG is determined by the multi-mass model of SG (free mode), the corresponding simulation results are shown in Figures 21 - 24.

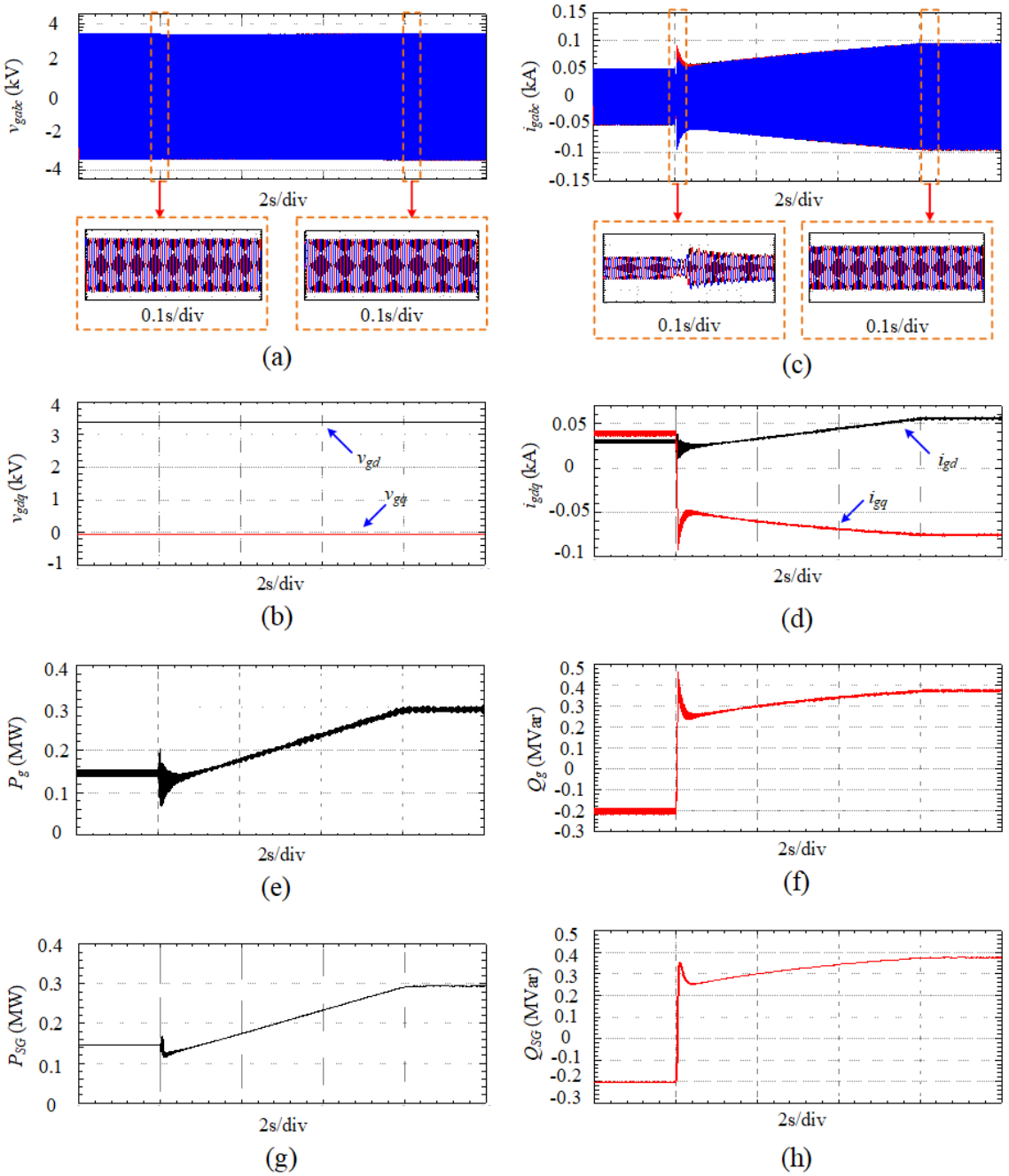

Figure 21: Simulation results for the SG variables by turning on the GSC control at 2s in the free mode (a) three-phase grid voltages; (b) dq grid voltages; (c) three-phase grid currents; (d) dq grid currents; (e) grid active power; (f) grid reactive power; (g) SG output active power; (h) SG output reactive power

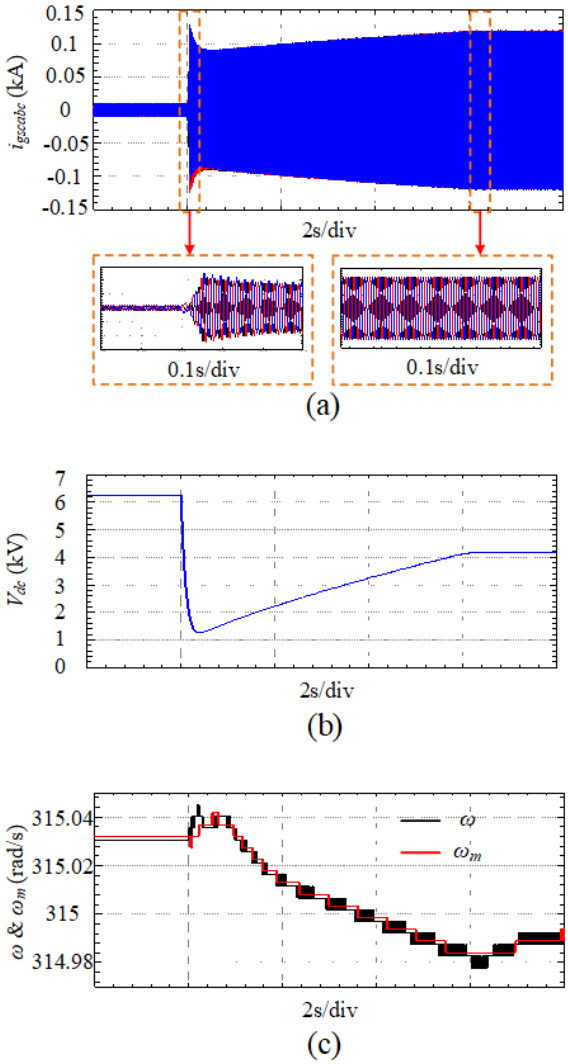

Figure 22: Simulation results for the variables of GSC with an SG power supply by turning on the GSC control at 2s in the free mode (a) three-phase GSC currents; (b) DC-bus voltage; (c) synchronous angular speed ω and SG rotor speed ω_m

It can be seen from Figures 21 and 22 that when the free mode is applied, there are fewer noises in the grid currents and power. In addition, the synchronous angular speed can precisely track the rotor speed of SG.

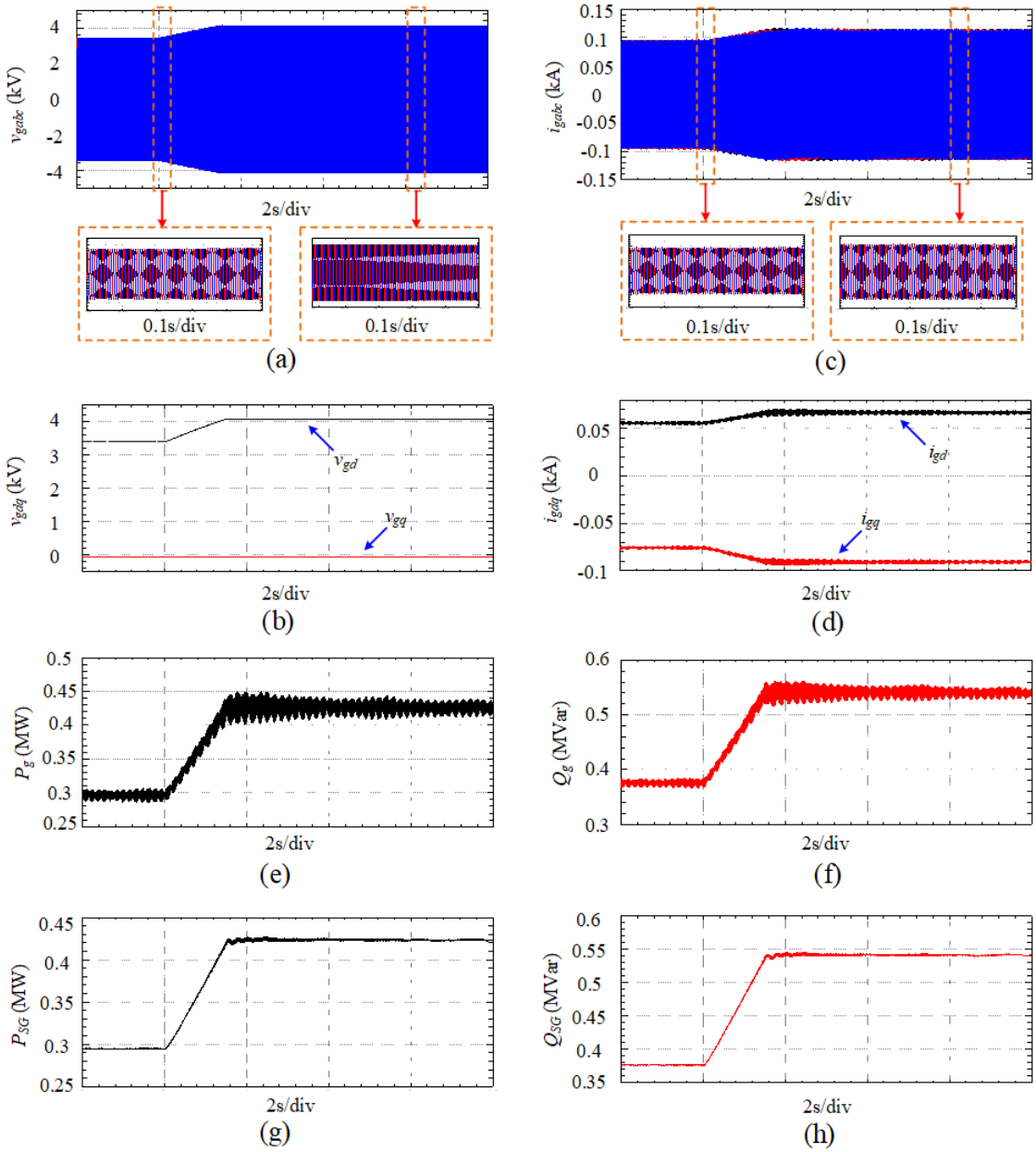

Figure 23: Simulation results for the SG variables by changing the exciter gain from 1 to 1.2 at 2s with the actual rotor angular speed (a) three-phase grid voltages; (b) dq grid voltages; (c) three-phase grid currents; (d) dq grid currents; (e) grid active power; (f) grid reactive power; (g) SG output active power; (h) SG output reactive power

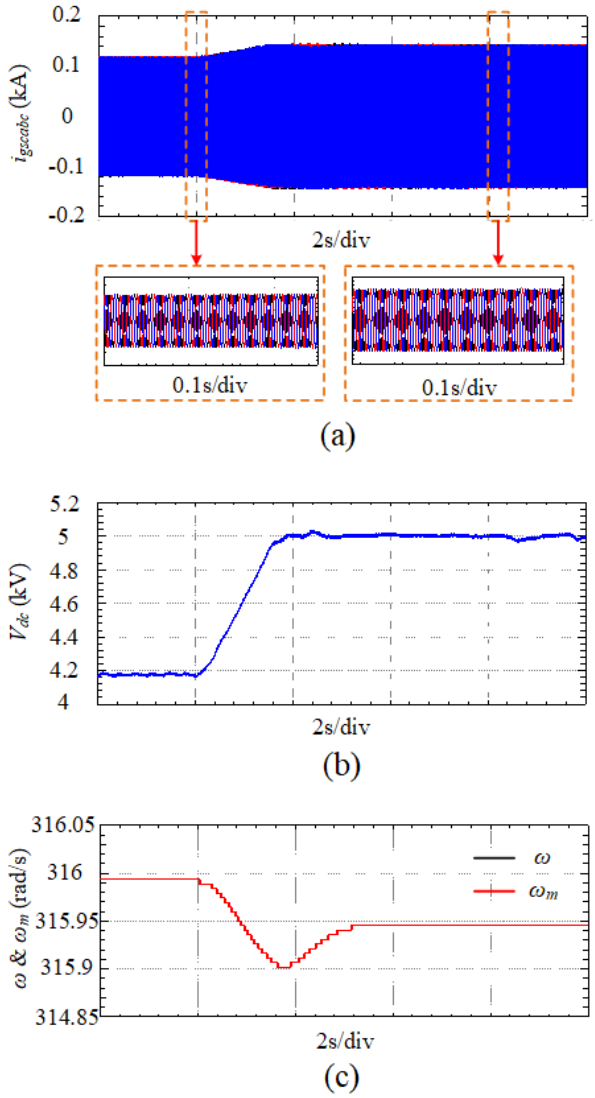

Figure 24: Simulation results for the variables of GSC with an SG power supply by changing the exciter gain from 1 to 1.2 at 2s with the actual rotor angular speed (a) three-phase GSC currents; (b) DC-bus voltage; (c) synchronous angular speed ω and SG rotor speed ω_m

After increasing the exciter gain from 1 to 1.2, the magnitudes of three-phase voltages, currents and DC-bus voltage increase, and the performance of the system is similar to the previous case, as is shown in Figures 23 and 24.

5.4 Simulation Results for RSC Connected with A Three-Phase Voltage Source

The control of RSC is then evaluated by using constant DC-bus voltage supply to eliminate the power circuit at the GSC side. In the simulation, the slip is maintained at 0.2 so that the base frequency of the three-phase rotor voltages is 10Hz, and the ASM is assumed to operate at the subsynchronous operation mode. In this case, the currents flow from the RSC to the rotor (three-phase voltage source in the RTDS simulation). The tracking performance of RSC is verified by changing the reference values of the rotor dq currents. In the proposed system, the vector control is based on grid voltage orientation (GVO), where the d-axis rotor current is controlled to regulate the active power, and the q-axis rotor current is controlled to regulate the reactive power. The d-axis current i_{rd} is first changed from 0kA to 1kA to make the rotor active power P_r change from 0 to a positive value. Then, with i_{rd} remained at 0kA, the q-axis current i_{rq} varies from 0kA to 1kA to change the rotor reactive power. The simulation results are displayed in Figures 25 and 26.

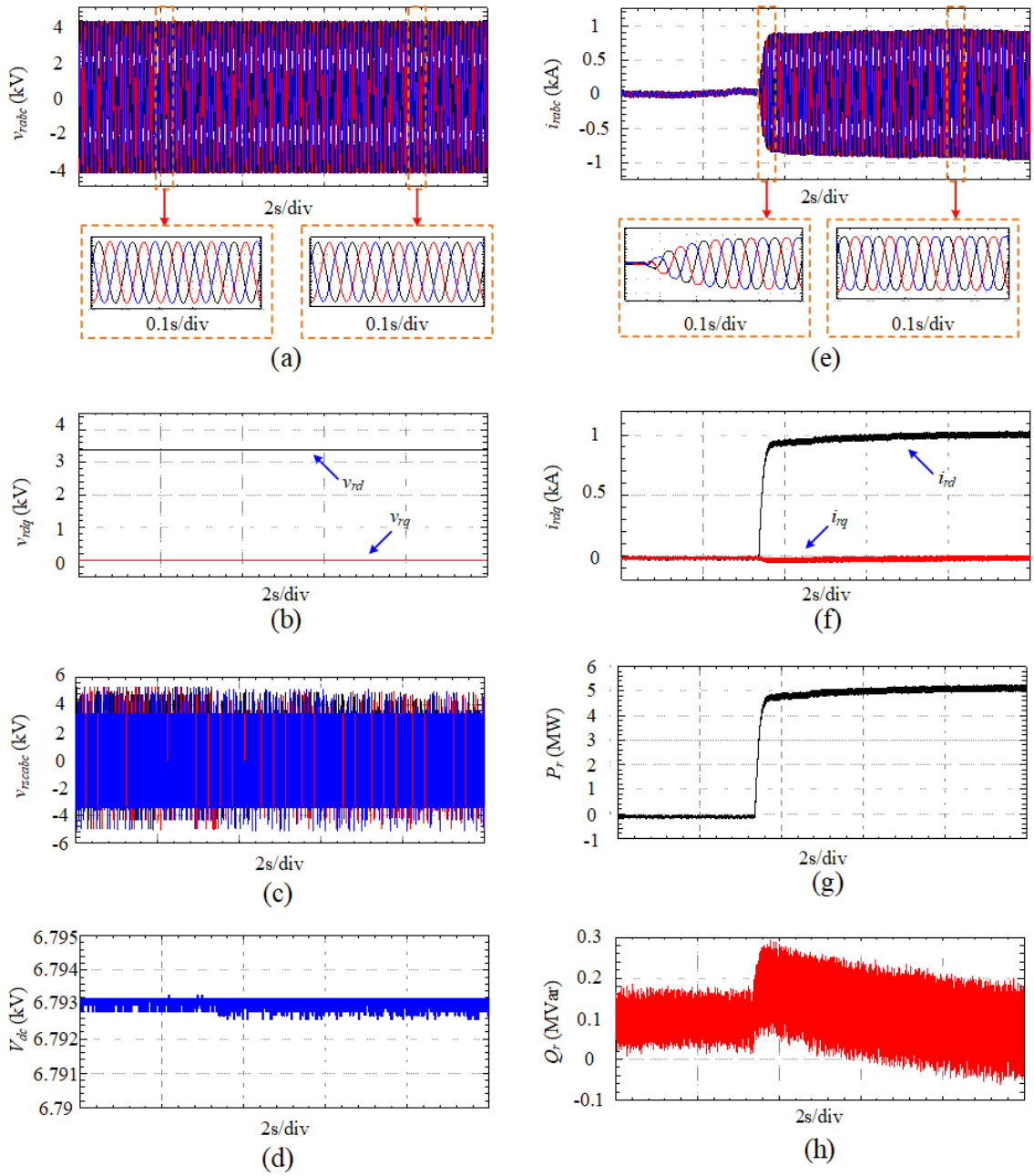

Figure 25: Simulation results for RSC connected with a three-phase voltage source with d-axis rotor current changing from 0 to 1kA at around 3.3s (a) three-phase rotor voltages; (b) dq rotor voltages; (c) three-phase RSC voltages; (d) DC-bus voltage; (e) three-phase rotor currents; (f) dq rotor currents; (g) rotor active power; (h) rotor reactive power

It can be seen from Figure 25 that with a constant DC-bus voltage supply, the control performance of RSC is satisfactory, and the rotor active power P_r increases at 3.3s with the change of i_{rd}, and it reaches 5MW at around 3.5s. Besides, the three-phase rotor current waveforms are almost sinusoidal, demonstrating a high current quality.

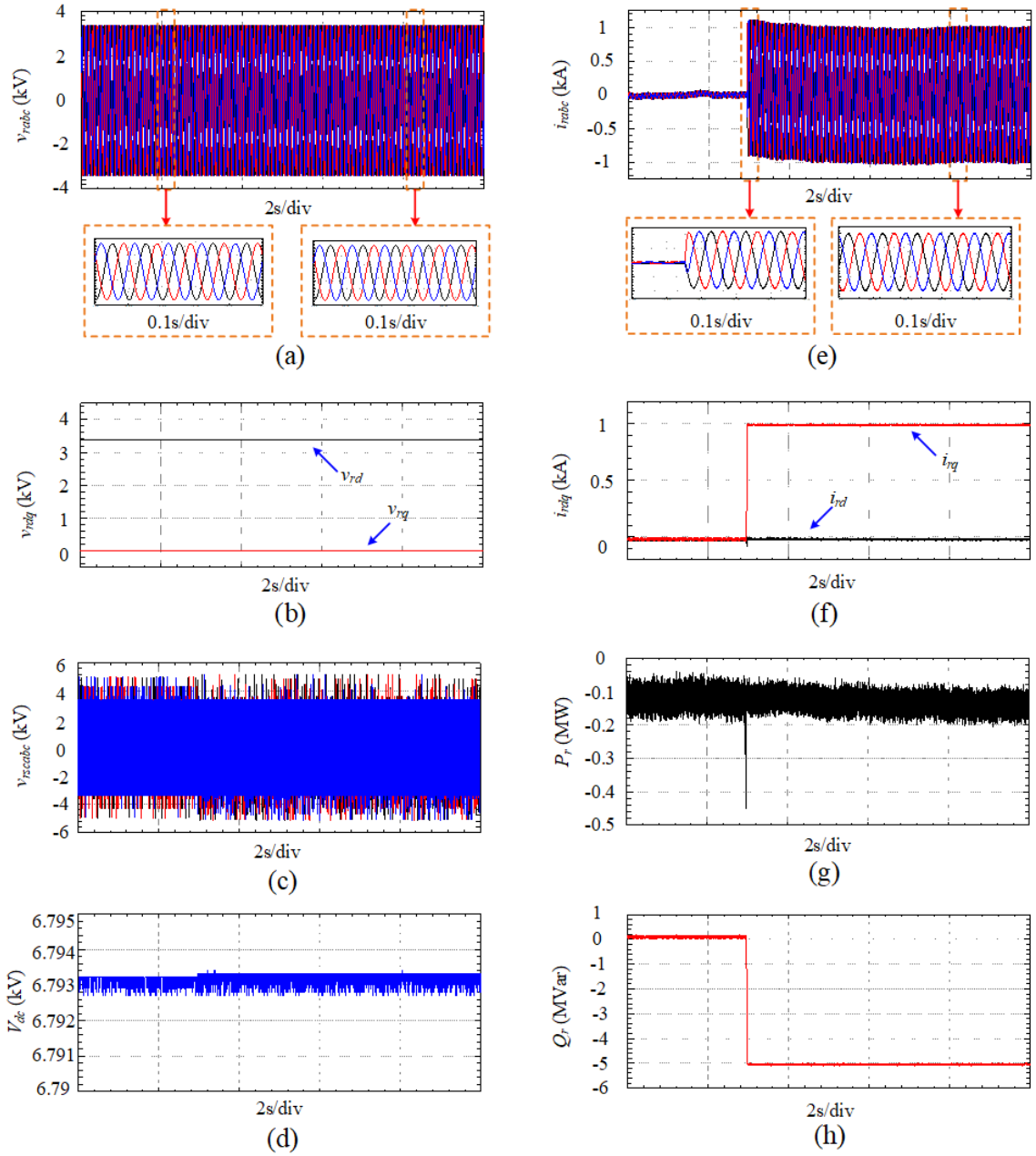

Figure 26: Simulation results for RSC connected with a three-phase voltage source with q-axis rotor current changing from 0 to 1kA at around 3.3s (a) three-phase rotor voltages; (b) dq rotor voltages; (c) three-phase RSC voltages; (d) DC-bus voltage; (e) three-phase rotor currents; (f) dq rotor currents; (g) rotor active power; (h) rotor reactive power

From Figure 26, similar performance to the case shown in Figure 25 can be observed. The three-phase rotor voltages and DC-bus voltage are stable, and the three-phase rotor currents are in almost sinusoidal waveforms. With the change in i_{rq}, the rotor reactive power Q_r changes instantly from 0 to -5MVar, as shown in Figure 26(h).

According to Figures 25 and 26, the tracking performance of RSC is fully verified for the proposed ASM-based SPS.

5.5 Simulation Results for SG Connected with BTB Converter

From Sections 5.1.2 to 5.1.4, the simulations were conducted for the GSC and RSC separately to verify their operation. In this section, the BTB converter that contains both GSC and RSC is applied

in the power circuit, and the control performance of the power circuit of SG connecting with BTB converter is to be verified. The exciter gain is kept at 1.2 and the control of GSC is on during the whole simulation process. The simulation results are displayed in Figures 27 – 29 by turning the RSC control on at 4s.

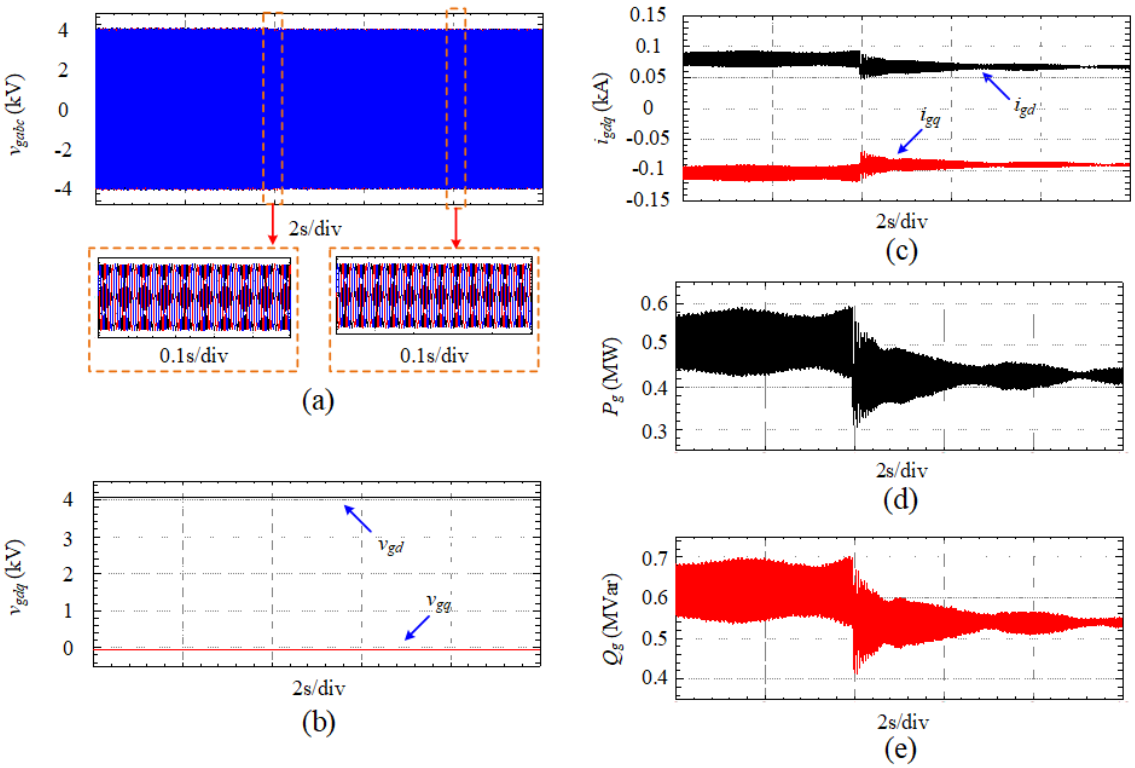

Figure 27: Simulation results for the SG variables in the power circuit of SG connected with BTB converter by turning the RSC control on at 4s (a) three-phase grid voltages; (b) dq grid voltages; (c) dq grid currents; (d) grid active power; (e) grid reactive power

It can be seen from Figure 27 that the grid voltages are stable during the whole process since it is simulated as an infinite power bus. There are some fluctuations in the dq grid currents, which result in the fluctuations in the grid active and reactive power.

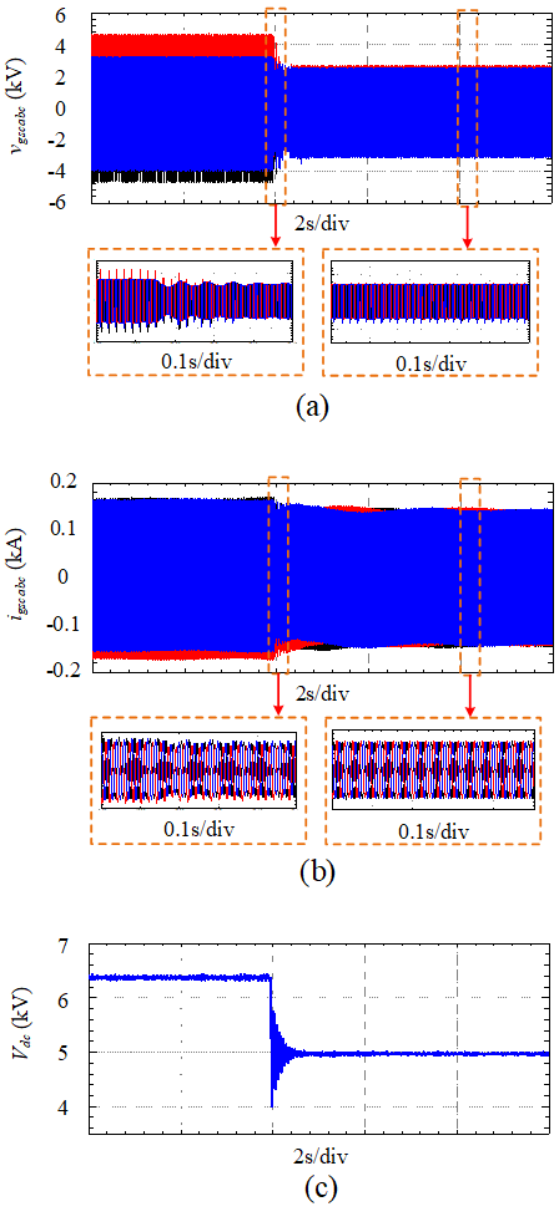

Figure 28: Simulation results for the GSC variables in the power circuit of SG connected with BTB converter by turning the RSC control on at 4s (a) three-phase GSC voltages; (b) three-phase GSC currents; (c) DC-bus voltage

From Figure 28, it can be seen that once the control of RSC is activated, the magnitude of DC-bus voltage declines from 6.4kV to 5kV. As a consequence, the magnitudes of GSC voltages and currents both decrease.

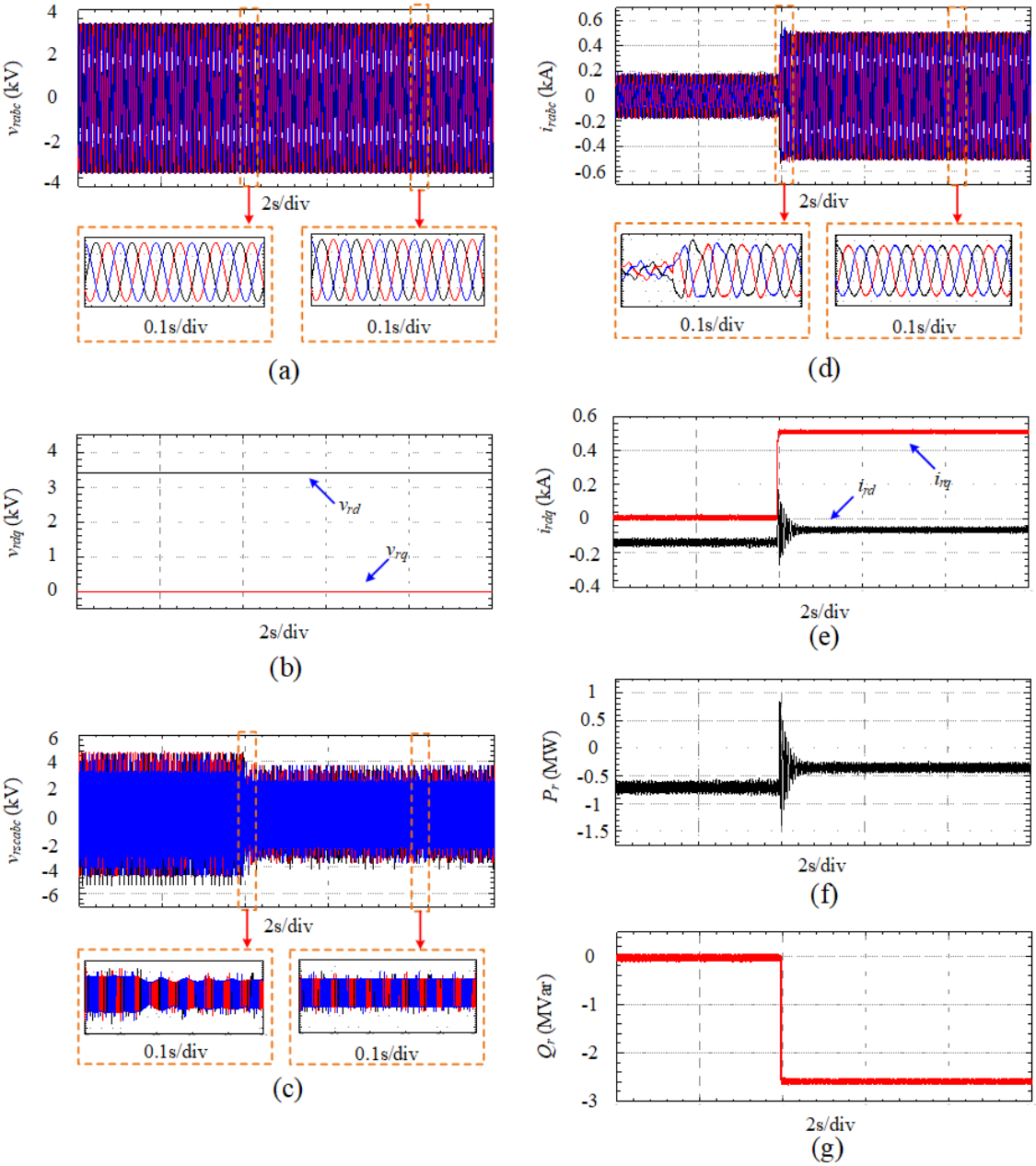

Figure 29: Simulation results for the rotor-side variables in the power circuit of SG connected with BTB converter by turning the RSC control on at 4s (a) three-phase rotor voltages; (b) dq rotor voltages; (c) three-phase RSC voltages; (d) three-phase RSC currents; (e) dq rotor currents; (f) rotor active power; (g) rotor reactive power

From Figure 29, it can be seen that the rotor voltages are always stable as the rotor of ASM is simulated as a constant three-phase voltage source. In addition, at the instant of activating the RSC control, the magnitude of three-phase RSC voltages drops, while that of three-phase rotor currents arises from 0.2kA to around 0.5kA, and almost sinusoidal current waveforms are presented. The reference values of i_{rd} and i_{rq} are set to 0kA and 0.5kA, respectively, and it can be clearly seen from Figure 29(e) that the dq rotor currents track these reference values appropriately. Moreover, the tracking performances of P_r and Q_r are verified in Figure 29(f) and (g).

5.6 Conclusion

The simulation results are derived by using RTDS with CHIL setup for the proposed ASM-based SPS. The rotor of ASM is simulated as a three-phase voltage source with the base frequency of the

slip frequency. The power circuit is simulated in separate parts first, and then these parts are combined to form the circuit of SG connected with a BTB converter. The following power circuits have been simulated in RTDS with the corresponding control strategies implemented in CHIL setup on the target PC: 1) three-phase voltage source feeding GSC; 2) SG connected with GSC; 3) RSC connected with a three-phase voltage source; 4) SG connected with BTB converter.

According to the simulation results, the following points are obtained.

1) Without considering the influence of SG parameters on the control performance of GSC, almost sinusoidal three-phase GSC currents can be obtained, and it takes around 4s for the variables of three-phase voltage source and GSC to reach the steady states.

2) When directly applying SG to connect with GSC, the three-phase grid voltages generated have high quality, therefore making the performance almost identical to the case in 1), in spite of some current ripples at the instant of enabling the GSC control and noises in the active and reactive power. Moreover, it takes longer time to achieve the steady operation.

3) After employing the free mode of controlling the SG connected GSC, fewer noises are presented in the grid currents and power.

4) Good tracking performances of rotor active and reactive power (transition period of shorter than 0.2s) are verified in the simulation studies for the power circuit of RSC connected with a three-phase voltage source, and the rotor current waveforms are almost sinusoidal.

5) When simulating the circuit of SG connected with BTB converter, the magnitudes of DC-bus voltage, GSC voltages, GSC currents, GSC active and reactive power, and RSC voltages all decrease at the point of enabling RSC control. On the other hand, the rotor-side variables are controlled well with high tracking performance.

To sum up, the controller design for GSC can be further improved to achieve better control performance, while the tracking performance of RSC is almost perfect for the proposed system.

6 Open Issues and Suggestions for Improvements

In this project, the operation of ASM-based SPS has been partially verified by simulating the power circuit of SG connected with BTB converter, without actually including the model of ASM. According to the simulation results obtained in RTDS with CHIL setup, there are some open issues, and improvements have to be conducted in the future works.

6.1 Open Issues

The control performance of GSC is not good enough according to the derived simulation results, since there are obvious fluctuations in the grid active and reactive power. In addition, the DC-bus voltage is not kept at the desirable value. The system model established in Simulink needs to be revisited and modified to improve the control performance of GSC. Then the RTDS models will be updated to control the system appropriately. In addition, the rotor speed of ASM is assumed to be a fixed value and the influence of load is not considered in this study.

6.2 Suggestions for Improvements

In the future work, the model of ASM will be added in the RTDS software, and the influence of the input mechanical torque for ASM will be considered to simulate a more practical case, as the wind speed constantly changes. Both the subsynchronous and supersynchronous operation modes for ASM will be implemented to verify the system performance. Furthermore, the fault scenario of grid voltage sag will be included to demonstrate that the system can still work properly with grid faults.

7 Dissemination Planning

According to the results obtained in this project, 1 journal article and 1 conference paper will be published, and further publication may be possible if both sides agree to cooperate in the future.
The experimental results will be added to our papers as important parts. We will take part in an IEEE conference to introduce our project and indicate the importance of it, and ask for advice from other researchers in similar research fields. Apart from that, we are going to invite them to deliver our ideas to their research institutions. After that, the paper will be published in IEEE journals to distribute our results to more researchers and students. Our results will be illustrated in posters and they will be displayed in our university. We will arrange visits and meetings to other universities and research institutions in the UK and in other countries to deliver our results by giving presentations and displaying our posters. In addition, the results of this proposed research will be involved in the training process for the undergraduate and MSC projects in University of Liverpool (UoL). These students will do their research based on the results of this work and they may further develop some new ideas to the existing results, which may help us improve the original method and produce a better prototype of the product. After the undergraduate and postgraduate students graduate from UoL, they will take these ideas into further education or work, and distribute the ideas to their colleagues, which leads to more discussion on this topic and create more ideas. We will keep in contact with these students and frequently communicate with them to discuss on this topic. Furthermore, we will collaborate with the researchers who are interested in this area, and we are going to continue working on this topic to produce more research achievements, and we will contact the corresponding enterprises to apply our technology in their products.

8 References

[1] A. Vicenzutti, D. Bosich, G. Giadrossi, G. Sulligoi, “The role of voltage controls in modern all electric ships, Toward the all electric ship, ” IEEE Electr. Mag., vol. 3, no. 2, pp. 49–65, 2015.

[2] Z. Wang, X. Wang, J. Cao, M. Cheng, Y. Hu, “Direct torque control of T-NPC inverters-fed double-stator-winding PMSM drives with SVM,” IEEE Trans. Power Electron., vol. 33, no. 2, pp. 1541–1553, 2018.

[3] P.-H. Wu, Y.-T. Chen, P.-T. Cheng, “The delta-connected cascaded H-bridge converter application in distributed energy resources and fault ride through capability analysis,” IEEE Trans. Ind. Appl., vol. 53, no. 5, pp. 4665–4672, 2017.

[4] M. Jankovic, A. Costabeber, A. Watson, J.C. Clare, “Arm-balancing control and experimental validation of a grid-connected MMC with pulsed DC load,” IEEE Trans. Ind. Electron., vol. 64, no. 12, pp. 9180–9190, 2017.

[5] Z. Quan, Y. Li, “Harmonic analysis of interleaved voltage source converters and tri-carrier PWM strategies for three-level converters,” 18th Workshop on Control and Modeling for Power Electronics (COMPEL), IEEE, Stanford, CA, USA, pp. 1–7, 2017.

[6] H. Liu, D. Zhang, D. Wang, “Design considerations for output capacitance under inductance mismatches in multiphase buck converters,” IEEE Trans. Power Electron., vol. 32, no. 7, pp. 5004–5015, 2017.

[7] E.A.R.E. Ariff, O. Dordevic, M. Jones, “A space vector PWM technique for a three-level symmetrical six-phase drive,” IEEE Trans. Ind. Electron., vol. 64, no. 11, pp. 8396–8405, 2017.

[8] H. Ma, G. Chen, J.H. Yi, Q.W. Meng, L. Zhang, J.P. Xu, “A single-stage PFM-APWM hybrid modulated soft-switched converter with low bus voltage for high-power LED lighting applications,” IEEE Trans. Ind. Electron., vol. 64, no. 7, pp. 5777–5788, 2017.

[9] T. Ericsen, N. Hingorani, Y. Khersonsky, “PEBB – power electronics building blocks. From concept to reality, Petroleum and Chemical Industry Conference,” 2006, PCIC ’06, Proc. IEEE Industry Applications Society 53rd Annual, Philadelphia, PA, USA, 2006, pp. 12–16.

[10] J. Yu, R. Burgos, N.R. Mehrabadi, D. Boroyevich, “DC fault current control of modular multilevel converter with SiC-based power electronics building blocks,” Electric Ship Technologies Symp., ESTS, IEEE, Arlington, VA, USA, pp. 30–35, 2017.

[11] F. Wang, Z. Zhang, T. Ericsen, R. Raju, R. Burgos, D. Boroyevich, “Advances in power conversion and drives for shipboard systems,” Proc. IEEE, vol. 103, no. 12, pp. 2285–2311, 2015.

[12] S. Debnath, J. Qin, B. Bahrani, M. Saeedifard, P. Barbosa, “Operation, control, and applications of the modular multilevel converter. A review,” IEEE Trans. Power Electron, vol. 30, no. 1, pp. 37–53., 2015.

[13] M.A. Perez, S. Bernet, J. Rodriguez, S. Kouro, R. Lizana, “Circuit topologies, modeling, control schemes, and applications of modular multilevel converters,” IEEE Trans. Power Electron., vol. 30, no. 1, pp. 4–17, 2015.

[14] R.M. Cuzner, R. Soman, M.M. Steurer, T.A. Toshon, M.O. Faruque, “Approach to scalable model development for navy shipboard compatible modular multilevel converters,” IEEE J. Emerg. Sel. Topics Power Electron., vol. 5, no. 1, pp. 28–39, 2017.

[15] R. Mo, H. Li, “Hybrid energy storage system with active filter function for shipboard MVDC system applications based on isolated modular multilevel DC/DC converter,” IEEE J. Emerg. Sel. Topics Power Electron. , vol. 5, no. 1, pp. 79–87, 2017.

[16] Y. Chen, S. Zhao, Z. Li, X. Wei, Y. Kang, “Modeling and control of the isolated DC-DC modular multilevel converter for electric ship medium voltage direct current power system,” IEEE J. Emerg. Sel. Topics Power Electron. , vol. 5, no. 1, pp. 124–139, 2017.

[17] P. Mitra, G.K. Venayagamoorthy, “An adaptive control strategy for DSTATCOM applications in an electric ship power system,” IEEE Trans. Power Electron. , vol. 25, no. 1, pp. 95–104, 2010.

[18] F.D. Kanellos, A. Anvari-Moghaddam, J.M. Guerrero, “A cost-effective and emission-aware

power management system for ships with integrated full electric propulsion," Electric Power Syst. Res., vol. 150, pp. 63–75, 2017.

[19] Y.D. Valle, G.K. Venayagamoorthy, S. Mohagheghi, J.C. Hernandez, R.G. Harley, "Particle swarm optimization. Basic concepts, variants and applications in power systems," IEEE Trans. E, Comput., vol. 12, no. 2, pp. 171–195, 2008.

[20] A. Karimi, A. Feliachi, "PSO-tuned adaptive backstepping control of power systems," Proc. IEEE Power Systems Conf. Expo., pp. 1315–1320, 2006.

[21] F. Zheng, Q. Wang, T.H. Lee, X. Huang, "Robust PI controller design for nonlinear systems via fuzzy modeling approach," IEEE Trans. Syst., Man, Cybern. A, Syst., Humans, vol. 31, no. 6, pp. 666–675, 2001.

[22] S. Mohagheghi, Y.D. Valle, G.K. Venayagamoorthy, R.G. Harley, "A proportional-integrator type adaptive critic design-based neurocontroller for a static compensator in multimachine power systems," IEEE Trans. Ind. Electron., vol. 54, no. 1, pp. 86–96, 2007.

[23] P. Kankanala, S.C. Srivastava, A.K. Srivastava, N.N. Schulz, "Optimal control of voltage and power in a multi-zonal MVDC shipboard power system," IEEE Trans. Power Syst., vol. 27, no. 2, pp. 642–650, 2012.

[24] S. Mashayekh, K.L. Butler-Purry, "An integrated security-constrained model-based dynamic power management approach for isolated microgrids in all-electric ships," IEEE Trans. Power Syst., vol. 30, no. 6, pp. 2934–2945, 2015.

[25] A.T. Abkenar, A. Nazari, S.D.G. Jayasinghe, A. Kapoor, M. Negnevitsky, "Fuel cell power management using genetic expression programming in all-electric ships," IEEE Trans. En. Conv., vol. 32, no. 2, pp. 779–787, 2017.

[26] F. Shariatzadeh, N. Kumar, A.K. Srivastava, "Optimal control algorithms for reconfiguration of shipboard microgrid distribution system using intelligent techniques," IEEE Trans. Ind. Appl., vol. 53, no. 1, pp. 474–482, 2017.

[27] Z. Jin, G. Sulligoi, R. Cuzner, L. Meng, J.C. Vasquez, J.M. Guerrero, "Next-generation shipboard DC power system. Introduction smart grid and DC microgrid technologies into maritime electrical networks," IEEE Electr. Mag., vol. 4, no. 2, pp. 45–57, 2016.

[28] F.D. Kanellos, "Optimal power management with GHG emissions limitation in all-electric ship power systems comprising energy storage systems," IEEE Trans. Power Syst., vol. 29, no. 1, pp. 330–339, 2014.

[29] F.D. Kanellos, G.J. Tsekouras, N.D. Hatziargyriou, "Optimal demand-side management and power generation scheduling in an all-electric ship," IEEE Trans. Sust. En., vol. 5, no. 4, pp. 1166–1175, 2014.

[30] T.A. Johansen, T.I. Bo, E. Mathiesen, A. Veksler, A.J. Sorensen, "Dynamic positioning system as dynamic energy storage on diesel-electric ships," IEEE Trans. Power Syst., vol. 29, no. 6, pp. 3086–3091, 2014.

[31] S. Mashayekh, K.L. Butler-Purry, "An integrated security-constrained model-based dynamic power management approach for isolated microgrids in all-electric ships," IEEE Trans. Power Syst., vol. 30, no. 6, pp. 2934–2945, 2015.

[32] IEEE recommended practice for 1 to 35kV medium voltage DC power systems on ships, 2010.

[33] C.-L. Su, K.-L. Lin, C.-J. Chen, "Power flow and generator-converter schemes studies in ship MVDC distribution systems," IEEE Trans. Ind. Appl., vol. 52, no. 1, pp. 50–59, 2016.

[34] X. Feng, K.L. Butler-Purry, T. Zourntos, "Multi-agent system-based real-time load management for all electric ship power systems in DC zone level," IEEE Trans. Power Syst., vol. 27, no. 4, pp. 1719–1728, 2012.

[35] M.M.S. Khan, M.O. Faruque, A. Newaz, "Fuzzy logic based energy storage management system for MVDC power system of all electric ship," IEEE Trans. En. Conv., vol. 32, no. 2, pp. 798–809, 2017.

[36] E.A. Sciberras, B. Zahawi, D.J. Atkinson, A. Breijs, J.H.V. Vugt, "Managing shipboard energy.

A stochastic approach special issue on marine systems electrification," IEEE Trans. Trans. Electr., vol. 2, no. 4, pp. 538–546, 2016.

[37] M.R. Banaei, R. Alizadeh, "Simulation-based modeling and power management of all-electric ships based on renewable energy generation using model predictive control strategy," IEEE Int. Trans. Syst. Mag., vol. 8, no. 2, pp. 90–103, 2016.

[38] P. Cairoli, R.A. Dougal, "New horizons in DC shipboard power systems. New fault protection strategies are essential to the adoption of DC power systems," IEEE Electr. Mag., vol. 1, no. 2, pp. 38–45, 2013.

[39] G. Sulligoi, D. Bosich, G. Giadrossi, L. Zhu, M. Cupelli, A. Monti, "Multiconverter medium voltage DC power systems on ships. Constant-power loads instability solution using linearization via state feedback control," IEEE Trans. Smart Grid, vol. 5, no. 5, pp. 2543–2552, 2014.

[40] M. JAKŠIĆ, Z. Shen, I. CVETKOVIĆ, D. Boroyevich, R. Burgos, C. Dimarino, F. Chen, "Medium-voltage impedance measurement unit for assessing the system stability of electric ships," IEEE Trans. En. Conv., vol. 32, no. 2, pp. 829–841, 2017.

[41] E. Christopher, M. Sumner, D.W.P. Thomas, X. Wang, F.D. Wildt, "Fault location in a zonal DC marine power system using active impedance estimation," IEEE Trans. Ind. Appl., vol. 49, no. 2, pp. 860–865, 2013.

[42] K.P. Logan, "Intelligent diagnostic requirements of future all-electric ship integrated power system," IEEE Trans. Ind. Appl., vol. 43, no. 1, pp. 139–149, 2007.

[43] P. Kotsampopoulos, D. Lagos, N. Hatziargyriou, M.O. Faruque, G. Lauss, O. Nzimako, P. Forsyth, M. Steurer, F. Ponci, A. Monti, V. Dinavahi, K. Strunz, "A Benchmark System for Hardware-in-the-Loop Testing of Distributed Energy Resources", IEEE Power and Energy Technology Systems Journal, vol. 5, no. 3, Sept. 2018

[44] M. Maniatopoulos, D. Lagos, P. Kotsampopoulos, N. Hatziargyriou, "Combined Control and Power Hardware-in-the-Loop simulation for testing Smart grid control algorithms", IET Generation, Transmission & Distribution, Vol. 11, Issue 12, August 2017

Annex

8.1 List of Figures

8.2 List of Tables